



INTERNATIONAL UNIVERSITY LIAISON INDONESIA (IULI)

BACHELOR'S THESIS

**A CONCEPTUAL DESIGN OF FLEXIBLE MISSION MALE: AERODYNAMICS
AND STABILITY**

By

Alibananda Tito Ash Shidiqui

11202001002

Presented to the Faculty of Engineering and Life Sciences
In Partial Fulfilment Of the Requirements for the Degree of

SARJANA TEKNIK

In

AVIATION ENGINEERING

FACULTY OF ENGINEERING AND LIFE SCIENCES

BSD City 15345

Indonesia

Month YEAR

APPROVAL PAGE

A CONCEPTUAL DESIGN OF FLEXIBLE MISSION MALE: AERODYNAMICS AND STABILITY

ALIBANANDA TITO ASH SHIDIQI

11202001002

Presented to the Faculty of Engineering

In Partial Fulfillment of the Requirements for the Degree of

SARJANA TEKNIK

In

AVIATION ENGINEERING

FACULTY OF ENGINEERING AND LIFE SCIENCES

Triwanto Simanjuntak, PhD

Thesis Advisor

Date

Dr. Eng. Ressa Octavianty

Thesis Co-Advisor

Date

Dipl.-Ing. Sentot Wahjoe Georitno, M.Si.

Dean of Faculty of Engineering and Life Sciences

Date

EXAMINERS APPROVAL PAGE

Name of Examiner 1

Examiner 1

Date

Name of Examiner 2

Examiner 2

Date

Name of Examiner 3

Examiner 3

Date

STATEMENT BY THE AUTHOR

I hereby declare that this submission is my own work and to the best of my knowledge, it contains no material previously published or written by another person, nor material which to a substantial extent has been accepted for the award of any other degree or diploma at any educational institution, except where due acknowledgement is made in the thesis.

Alibananda Tito Ash Shidiqi

Student

Date

ABSTRACT

A Conceptual Design of Flexible Mission MALE: Aerodynamics and Stability

by

Alibananda Tito Ash Shidiqi

Triwanto Simanjuntak, PhD, Advisor

Dr. Eng. Ressa Octavianty, Co-Advisor

This bachelor's thesis studied the conceptual design of a Medium Altitude Long Endurance (MALE) Unmanned Aerial Vehicle (UAV), with an emphasis on its aerodynamic performance and stability characteristics. MALE UAVs bridge the gap between High Altitude Long Endurance (HALE) and small tactical UAVs, making them not only cost-effective but also useful for a variety of military and civilian applications. The conceptual design of this UAV aimed to provide a versatile aerial platform that might serve as a viable alternative for MALE UAV development in Indonesia. The project began with an investigation of 22 lists of MALE UAVs, followed by the building and analysis of a conceptual design in Open VSP and XFLR5. The final design, created in Open VSP, proved stable UAV performance in all stability modes except spiral mode and could accommodate any payload combination.

Keyword: *Aircraft Design, MALE, UAV*

ACKNOWLEDGEMENTS

I wish to express my heartfelt gratitude to all individuals who have provided assistance and support over the course of my thesis completion. First and foremost, I want to express my praise and gratitude to Allah SWT for bestowing Allah's blessings upon this entire thesis, as well as granting us good health, resilience, and wisdom throughout its completion.

I would like to express my sincere appreciation to my thesis advisor and co-advisor Triwanto Simanjuntak, PhD, and Dr. Eng. Ressa Octavianty, for their invaluable mentorship, assistance, and motivation over the course of my studies.

Their insightful ideas, suggestions, and expertise assisted me in refining both myself and this thesis into a better version. Despite experiencing periods of lack of motivation, they consistently assist me in regaining focus and maintaining the drive necessary to complete my thesis. I am immensely grateful to them for dedicating their time and energy to support me as my thesis supervisor, despite their other obligations.

I'd want to thank my colleagues and friends for their support and encouragement during difficult moments. Their encouragement helps me stay motivated and focused on completing this thesis. Finally, I would want to thank my family, particularly my parents, for their unwavering love, support, and encouragement in any manner. Their dedication and faith in me have been important in allowing me to reach this point in my life and academic journey.

I want also to express my utmost gratitude to Dewi Habsari Budiarti, PhD, and Siti Vivi Octaviany, S.T., M.T. for their invaluable contributions as examiners for my thesis.

I am grateful to everyone who contributed in some manner to the completion of this thesis. This accomplishment would not have been possible without the help and encouragement of everyone who believed in me. Thank you everybody for your fantastic, priceless assistance and contributions.

Contents

Approval Page	i
EXAMINERS APPROVAL PAGE	ii
Statement by The Author	iii
Abstract	iv
Acknowledgements	v
Contents	vi
List of Figures	ix
List of Tables	xi
1 Introduction	1
1.1 Background	1
1.2 Problem Statement	2
1.3 Research Objectives	2
1.4 Research Scope and Limitation	2
1.5 Significance of the Study	3
2 Literature Review	4
2.1 MALE UAV	4
2.1.1 Introduction to UAV	4
2.1.2 MALE UAV Definition	5
2.2 Aerodynamic Basis	6
2.2.1 Wing and Tail Geometrical Characteristic	6

2.2.2	Aerodynamic Forces and Moments	7
2.3	Equation of Motion	9
2.3.1	EOM of a Rigid Symmetric Aircraft	9
2.3.2	Linearised EOM	10
2.3.3	Gravitational Terms	11
2.3.4	Aerodynamics Terms	12
2.3.5	Aerodynamics Control Terms	13
2.3.6	Power Terms	14
2.3.7	EOM for Small Perturbations	15
2.4	Aircraft Stability	16
2.4.1	Modes of Aircraft Motion	17
2.4.2	Reference Axes	18
2.4.3	Static Stability and Dynamic Stability	19
2.4.4	Characteristic Equations	22
2.4.5	Root Mapping on the S-Plane	24
2.5	Previous Work	25
2.5.1	P.Panagioutou et al., 2016 [14]	25
2.5.2	Zdobyslaw Goraj, 2004 [15]	26
2.5.3	Ashish Karki et al., 2021 [16]	27
2.5.4	A. Septiyana et al., 2020 [17]	28
3	Research Methodology	30
3.1	Conceptual Design Process Flowchart	30
3.2	Benchmarking Study	31
3.3	Mission Profile and Design Requirements	31
3.3.1	Design Requirements	32
3.3.2	Mission Profile and Target Performance	33
3.4	Modelling in OpenVSP	33
3.4.1	Introduction to OpenVSP	33
3.4.2	Fuselage	34
3.4.3	Airfoil	35
3.4.4	Wing Modelling	35
3.4.5	Tail Modelling	37

3.5	Modeling in XFLR5	38
3.5.1	Introduction to XFLR5	38
3.5.2	Wing and Tail Shape Modelling	38
3.5.3	Mass Input	41
4	Results and Discussions	42
4.1	Weight Estimation	42
4.2	Mass Input in XFLR5	42
4.3	Aerodynamic Analysis	44
4.3.1	Configuration Selection	44
4.3.2	Fuselage	45
4.3.3	Airfoil	47
4.3.4	Wing	50
4.3.5	Tail	51
4.3.6	Total Parasite Drag	54
4.4	Static Stability Analysis	55
4.5	Dynamic Stability Analysis	56
4.5.1	Longitudinal Modes	58
4.5.2	Lateral Modes	60
4.5.3	S-Plane	60
5	Summary, Conclusion, Recommendation	65
5.1	Summary	65
5.2	Conclusion	65
5.3	Recommendation	66
	Bibliography	67
	Appendices	70
.1	Dynamic Stability Output	71
.2	Benchmarking Table	75
	Turnitin Report	80
	Curriculum Vitae	82

List of Figures

2.1	Classification of UAV based on operating altitude from [7].	6
2.2	Wing geomtery reprinted from [8].	7
2.3	Resultant force components split reprinted from [9].	8
2.4	Aircraft Motion.	18
2.5	Reference axes.	19
2.6	Longitudinal Stability.	20
2.7	Lateral-Directional Stability.	21
2.8	Illustration of static stability reprinted from [13].	22
2.9	Stability Comparison reprinted from [10].	23
2.10	Illustration of Degree of Stability reprinted from [10].	24
2.11	Splan reprinted from [10].	24
3.1	Research Methodology	30
3.2	Mission Profile	33
3.3	Fuselage Models	35
3.4	NLF 0215	35
3.5	NLF 0415	35
3.6	NACA 23015	35
3.7	NACA 64215	35
3.8	Airfoils Candidate	35
3.9	Plan tab menu	36
3.10	Section tab menu	36
3.11	Airfoil menu	36
3.12	Wing shape	36
3.13	Parameter setting	36
3.14	Tail Modelling	37

3.15 Airfoil Design	39
3.16 Airfoil Analysis	39
3.17 Wing	40
3.18 Tail Upper	40
3.19 Tail Lower	40
3.20 3D Shape Wing and Tail	40
3.21 Mass Input	41
4.1 Parts Location	44
4.2 Mass Points	45
4.3 Three Wing Configuration	46
4.4 Fuselage Dimension	47
4.5 CL VS Alpha	48
4.6 CL VS Cd	48
4.7 Cm VS Alpha	48
4.8 CL/CD VS CL	48
4.9 Airfoil Aerodynamic Characteristics	48
4.10 Induced Drag Factor versus Taper Ratio and Aspect Ratio [20].	50
4.11 Estimation CL Maximum of the Wing.	51
4.12 Upper X-tail.	53
4.13 Lower X-tail.	54
4.14 Final lower and upper X-tail area.	54
4.15 Geometric Shape of the X-Tail.	55
4.16 Static Stability.	57
4.17 Longitudinal Modes.	59
4.18 Lateral Modes.	61
4.19 Root Locus View of Longitudinal Modes.	63
4.20 Root Locus View of Lateral Modes.	64

List of Tables

4.1 Payload Weight 43

4.2 Structural Weight 43

4.3 Software calculation differences 46

4.4 Scoring table fuselage 46

4.5 Airfoil Matrix. 49

4.6 Wing Parameters. 51

4.7 Tail Volume Table Reprinted from [23]. 52

4.8 Conventional Tail Area from Tail Volume GA Single Engine. 53

4.9 V-Tail Volume 53

4.10 Total Parasite Drag. 56

4.11 Static Stability. 56

List of Abbreviations

UAV	Unmanned Aerial Vehicle
CFD	Computational Fluid Dynamics
FEA	Finite Element Analysis
UAV	Unmanned Aerial Vehicle
COG	Center of Gravity
CAD	Computer Aided Design
RPM	Rotation Per Minute
EOM	Equation of Motion
MALE	Medium Altitude Long Endurance
HALE	High Altitude Long Endurance
CM	Coefficient of Moment
CL	Coefficient of Lift
CD	Coefficient of Drag
Cl	Coefficient of Rolling Moment
Cn	Coefficient of Yawing Moment
CG	Center of Gravity
MTOW	Maximum Takeoff Weight
COTS	Commercial Off the Shelf
SAR	Search and Rescue
ISR	Intellegence Surveillance Reconnaissance

Dedicated to my parents

CHAPTER 1

INTRODUCTION

1.1 Background

According to Frederick et al. (1993) [1], Indonesia is an archipelagic nation that spans a distance of 1,760 kilometers (1,094 miles) from north to south and 5,120 kilometers (3,181 miles) from east to west. It is also one of the biggest archipelagic countries in the world, consisting of 17,500 islands, according to a geospatial study undertaken between 2007 and 2010 by the National Coordinating Agency for Study and Mapping (Bakosurtanal) [2]. The distinctive geographical and strategic qualities of an archipelagic nation such as Indonesia, which possesses a huge coastline and many islands, create an increased demand for MALE UAVs. Due to the capabilities of these aircraft, they have the potential to be an essential choice for Indonesia's security. As a result of the fact that medium-altitude operations offer flexibility for a wide range of tasks, ranging from military to civilian, including search and rescue, scientific missions, surveillance, intelligence, and even warfare, the development of the MALE unmanned aerial vehicle (UAV) is significant for Indonesia. According to [3], Indonesia has been collaborating with a group of six institutions, which includes the Ministry of Defense, PT Dirgantara Indonesia, ITB, the Agency for the Assessment and Application of Technology (BPPT), the Indonesian Air Force, and PT LEN Persero, in order to develop the Medium Altitude Long Endurance (MALE) unmanned aerial vehicle (UAV) known as Elang Hitam. This development was initiated by the Ministry of Defense's Research and Development in 2015. The unmanned aerial vehicle (UAV) prototype was presented to the public on December 30, 2019, in the hangar of PT Dirgantara Indonesia in Bandung, West Java. It is anticipated that the unmanned aerial vehicle (UAV) would be able to carry missiles and will

be able to cruise at heights of up to 23,000 feet for up to 30 hours in a row. Therefore, as of the 15th of September in the year 2022, the development of the drone has been placed on hold [4]. This conceptual design of the MALE UAV is designed to fill in the design choices of the MALE UAV in Indonesia, which acts as an alternate design choice in addition to the Elang Hitam design.

1.2 Problem Statement

To cover the unique geographical characteristics of Indonesia such as a lengthy border with different kind of terrain, Indonesia can't always rely on human power because this kind of mission is a type of dull mission that is high risk of human factor problems. one of the solutions is Indonesia needs to seek an efficient method to do such assignment. One of the solutions is to develop our own MALE UAV so that Indonesia can securely protect its border without any dependencies with other countries and it is also more cost-effective in comparison to buying UAVs from other countries in the long term.

1.3 Research Objectives

The objectives of this research are to investigate:

- To create a cutting-edge MALE-UAV capable of performing a variety of multirole missions.
- To create a UAV as an alternate design for Indonesia beside Elang Hitam UAV.

1.4 Research Scope and Limitation

In this study it only represents the aerodynamic and stability of the conceptual design MALE UAV. For the structural design, mission avionics, and payloads system are covered by my colleague Mr. Akbar Lazuardy Ikhsan.

1.5 Significance of the Study

The results of this research are expected:

- Can be used as an alternative design choice of MALE UAV development in Indonesia.
- The aerodynamic performance of this Conceptual MALE UAV can compete with others MALE UAVs.
- This conceptual UAV can be stable in each stability modes without the help of the stability augmentation system.

CHAPTER 2

LITERATURE REVIEW

2.1 MALE UAV

2.1.1 Introduction to UAV

In the realm of modern technology, Unmanned Aerial Vehicles (UAVs) have emerged as revolutionary instruments, reshaping the landscape of various industries and pushing the boundaries of what is possible in the skies. UAVs represent a paradigm shift in aviation, eliminating the need for onboard human pilots and offering a diverse range of applications across sectors such as military, commercial, scientific research, and recreational pursuits.

At their core, UAVs are autonomous or remotely piloted aircraft that navigate through the air without a human pilot on board. This autonomy is made possible by advanced technologies such as GPS (Global Positioning System), sophisticated sensors, and cutting-edge communication systems. UAVs come in various shapes and sizes, from small quadcopters suitable for recreational use to large, high-altitude drones designed for surveillance or cargo delivery.

The military was an early adopter of UAV technology, employing drones for reconnaissance, surveillance, and even combat missions. The mission employment were based on "3D" concept which means dull, dirty and dangerous [5]. Dull refers to extended-duration missions that may extend over multiple days in the future. Dirty refers to tasks involving the identification and measurement of chemical substances, which should be avoided in manned missions if feasible. However, the scope of UAV applications has expanded dramatically, infiltrating industries like agriculture, environmental monitoring, infrastructure inspection, and filmmaking. In agriculture, for instance, UAVs equipped with cameras and

sensors can assess crop health, optimize irrigation, and monitor overall field conditions with unparalleled precision.

In recent years, the word unmanned aerial vehicle (UAV) has gained significant popularity. However, there is currently a movement to replace this term with unmanned aircraft system (UAS). The primary distinction is in the utilisation of the term "aircraft," which signifies the requirement for airworthiness certification. Furthermore, a UAS is currently defined as a comprehensive "system" encompassing not only the "UAV" itself, but also the launch and recovery system, the ground control station, and the communication link [6].

2.1.2 MALE UAV Definition

Based on parameters such as flight range, flight altitude, and load capacity, UAVs can be divided into five types: High-altitude long-endurance (HALE) UAVs, Medium-altitude long-endurance (MALE) UAVs, Tactical UAVs (TUAV), Small UAVs (SUAV) Miniature UAVs (MAV)[7].

However, the main distinction between these types is the operational altitude. Medium-altitude long-endurance UAVs are commonly operated in class A airspace, which is around 20000- 60000 ft (6096-18288 meters) [7].

One defining feature of MALE UAVs is their capability to operate at medium altitudes, which provides them with advantages in terms of both surveillance and endurance. The altitude range allows them to maintain a broader perspective over a designated area, making them well-suited for intelligence, surveillance, reconnaissance (ISR), and target acquisition missions. This altitude range strikes a balance between maintaining a safe distance from potential threats and ensuring effective data collection and communication capabilities.

Medium Altitude Long Endurance UAVs are equipped with advanced sensor systems, communication tools, and often carry a payload for various purposes, including high-resolution cameras, infrared sensors, and other reconnaissance equipment. The extended endurance capability enables these UAVs to remain airborne for prolonged periods, facilitating persistent monitoring and data collection without the need for frequent refueling or recharging.

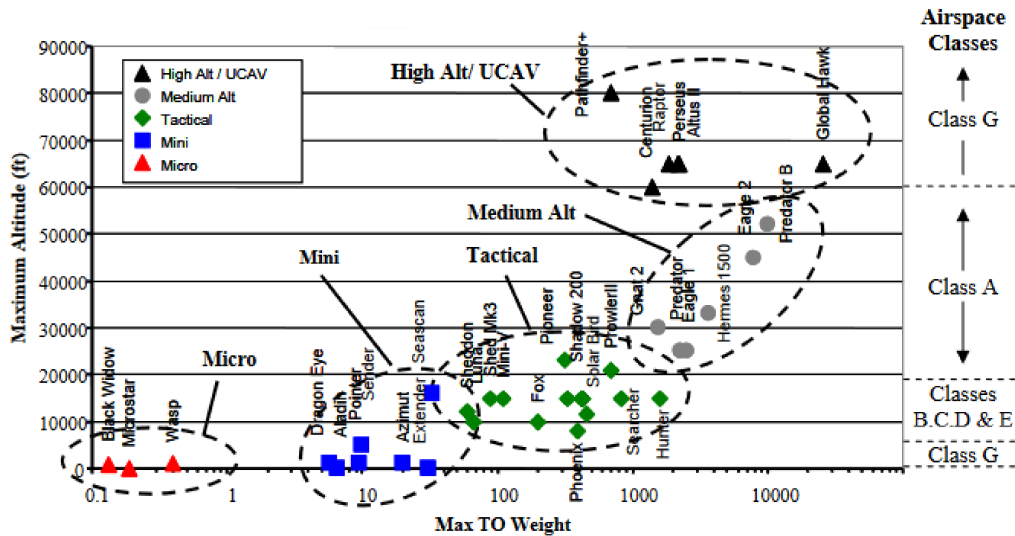


FIGURE 2.1: Classification of UAV based on operating altitude from [7].

2.2 Aerodynamic Basis

2.2.1 Wing and Tail Geometrical Characteristic

The most critical part of aircraft is the wing. It provides the main lift source so that it must be carefully designed in order to optimize its performance. The figure 2.2 shows all of the main parameter of wing and tail geometry.

- C_T = Tip chord of wing
- C_0 = Root chord of wing, in other text book $C_0 = C_r$
- S = Wing plan area
- λ = Wing taper ratio, C_T/C_0
- b = Wing span
- A or AR = b^2/S
- t/c = Wing thickness chord ratio, maximum local thickness divided by chord length
- α = Geometric angle of attack
- MAC = Mean aerodynamic chord

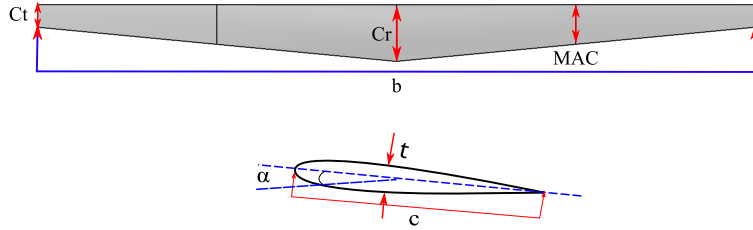


FIGURE 2.2: Wing geomtery reprinted from [8].

2.2.2 Aerodynamic Forces and Moments

The aerodynamic forces and moments are solely attributed to two primary sources: the pressure distribution p and the shear stress distribution τ . The combined outcome of these factors is a resultant force, denoted as R , and a moment, denoted as M , acting on the body. According on the Figure 2.3, the resultant force is divided into several component, namely :

based on the figure above, resultant force is split into several components, namely:

- V_∞ = Freestream velocity
- $L \equiv$ lift \equiv component of R perpendicular to V_∞
- $D \equiv$ drag \equiv component of R parallel to V_∞
- $N \equiv$ normal force \equiv component of R perpendicular to c
- $A \equiv$ axial force \equiv component of R parallel to c

with the angle of attack is located between c and V_∞ , Hence, α defined as angle between L and N and between D and A .

- $L = N \cos \alpha - A \sin \alpha$
- $D = N \sin \alpha + A \cos \alpha$

The lift and drag forces are commonly expressed as dimensionless coefficients, as stated in equations below. The wing reference area, often known as S_{ref} or

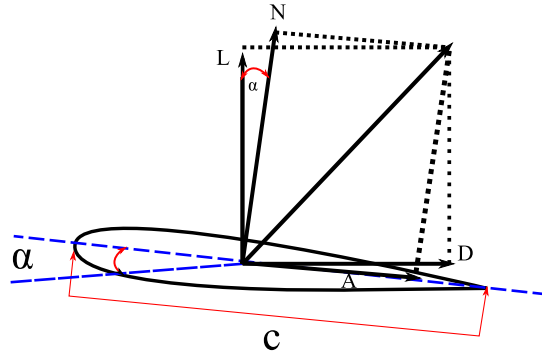


FIGURE 2.3: Resultant force components split reprinted from [9].

simply S , refers to the area region that extends up to the centerline of the aircraft. The freestream air's dynamic pressure is referred to as q .

$$L = qSC_L \quad (2.1)$$

$$D = qSC_D \quad (2.2)$$

Where

$$q = \frac{1}{2}\rho V^2 \quad (2.3)$$

C_L with uppercase subscripts means three-dimensional wing, on the other hand, lower case subscripts means C_l two-dimensional airfoil characteristics.

Uncambered :

$$C_D = C_{D0} + KC_L^2 \quad (2.4)$$

Cambered :

$$C_D = C_{Dmin} + K(C_L - C_{Lmindrag})^2 \quad (2.5)$$

CL/CD is one of the most important aspect in term designing aircraft. CL/CD is increased relative to the increasing angle of attack, but at one point the CL/CD reaches its maximum value. This maximum value called (L/D)max which is equal to (CL/CD)max. This value is a direct measure of aerodynamic efficiency of an airplane, therefore this value is an important value in airplane design and also the airplane performance itself

2.3 Equation of Motion

2.3.1 EOM of a Rigid Symmetric Aircraft

The equations of motion for a rigid symmetric aircraft are essential for comprehending its dynamic characteristics. The equations are derived from Newton's second law of motion. The law of motion, known as Newton's second law, states that the force exerted on an object is directly proportional to the product of its mass and acceleration ($F = ma$). During the flight of an aeroplane, this approach is utilised to address all six degrees of freedom that the aircraft can undergo: three linear motions (forward/backward, vertical, lateral) and three rotating motions (roll, pitch, yaw). In rotational motion, forces are substituted with moments (torques), mass is replaced by moment of inertia, and linear acceleration substituted for angular acceleration. The equations are classified into two primary categories: Equation 2.6 represents the equations for translational motion. The equations provided depict the linear movement of the aircraft's centre of gravity (cg) along the body-fixed axes (ox, oy, oz).

$$\begin{aligned} m(\dot{U} - rV + qW) &= X_a + X_g + X_c + X_p + X_d \\ m(\dot{V} - pW + rU) &= Y_a + Y_g + Y_c + Y_p + Y_d \\ m(\dot{W} - qU + pV) &= Z_a + Z_g + Z_c + Z_p + Z_d \end{aligned} \quad (2.6)$$

Noted that (m) is the mass of the aircraft, $(\dot{U}, \dot{V}, \dot{W})$ are the body-axis components of linear acceleration, (p, q, r) are the angular velocity components about the body axes, and (X, Y, Z) are the forces along the respective axes. The subscripts denote the source of the forces: aerodynamic (a), gravitational (g), control (c), powerplant (p), and disturbance (d).

Rotational Motion Equations (Equation 2.7): These equations describe the rotational motion about the body axes and are given by:

$$\begin{aligned} I_x \dot{p} - (I_y - I_z)qr - I_{xz}(pq + \dot{r}) &= L \\ I_y \dot{q} + (I_x - I_z)pr + I_{xz}(p^2 - r^2) &= M \\ I_z \dot{r} - (I_x - I_y)pq + I_{xz}(qr - \dot{p}) &= N \end{aligned} \quad (2.7)$$

where (I_x, I_y, I_z) are the moments of inertia about the respective axes, $(\dot{p}, \dot{q}, \dot{r})$ are the angular accelerations, and (L, M, N) are the moments about the respective axes.

2.3.2 Linearised EOM

To analyse the equations of motion (EOM), linearization is necessary. Linearization can be accomplished by restricting the aircraft's motion to minor disturbances around the trim state. The chosen reference state for linearization is a state of steady trimmed rectilinear flight, in which the aeroplane is maintaining a straight and level trajectory with a constant velocity and no angular movement. This indicates that the aeroplane is in a state of balance, where all forces and moments are evenly distributed. The velocity components along the body-fixed axis are (U_e, V_e) and (W_e) , with $(V_e = 0)$ because there is no sideways movement. Additionally, all angular velocity components are zero. Given that the velocity V_e is equal to zero, it implies that there are no external forces or moments causing disturbances on the aircraft:

$$X_d = Y_d = Z_d = L_d = M_d = N_d = 0 \quad (2.8)$$

The linearized equations of motion can be expressed as follows:

$$\begin{aligned} m(\dot{u} + qW_e) &= X_a + X_g + X_c + X_p \\ m(\dot{v} - pW_e + rU_e) &= Y_a + Y_g + Y_c + Y_p \\ m(\dot{w} - qU_e) &= Z_a + Z_g + Z_c + Z_p \end{aligned} \quad (2.9)$$

Here, (m) is the mass of the aircraft, $(\dot{u}, \dot{v}, \dot{w})$ are the linear disturbance velocities, and (p, q, r) are the angular disturbance velocities. The terms (X_a, Y_a, Z_a) represent the aerodynamic forces, (X_g, Y_g, Z_g) are the gravitational forces, (X_c, Y_c, Z_c) are the control forces, and (X_p, Y_p, Z_p) are the propulsion forces.

The linearized equations assume that the disturbance velocities and angular velocities are small, so terms involving their products and squares can be neglected. This simplification allows for the analysis of the aircraft's response to small disturbances and the design of control systems to enhance stability and performance. The linearized equations form the basis for understanding the dynamic behavior of the aircraft near the trimmed flight condition and are essential for the study of aircraft stability and control.

2.3.3 Gravitational Terms

The gravitational terms in the linearized equations of motion for an aircraft experiencing small perturbations from a steady, trimmed flight condition. The gravitational force, denoted by (mg) (where (m) is the mass of the aircraft and (g) is the acceleration due to gravity), is resolved into components along the body-fixed axes of the aircraft. These components contribute to the motion of the aircraft when it is disturbed from its equilibrium state.

The gravitational force components in the small perturbation equations of motion are given by the following equations:

$$\begin{aligned} X_g &= -mg \sin \theta_e - mg\theta \cos \theta_e \\ Y_g &= mg\psi \sin \theta_e + mg\phi \cos \theta_e \\ Z_g &= mg \cos \theta_e - mg\theta \sin \theta_e \end{aligned} \quad (2.10)$$

Here, (θ_e) is the pitch angle in the equilibrium state, (ϕ) is the roll angle, and (ψ) is the yaw angle. The terms (θ, ϕ, ψ) represent small angular perturbations about the equilibrium state. The document notes that since the aircraft is initially flying wings level, the weight components only appear in the plane of symmetry, and there are no weight moments about any of the axes, hence $(L_g = M_g = N_g = 0)$.

2.3.4 Aerodynamics Terms

The aerodynamic terms in the linearized equations of motion address the changes in aerodynamic forces and moments when an aircraft is disturbed from its equilibrium state. These changes are complex due to the intricate interactions between the aircraft's motion and the airflow around it. The method for describing these aerodynamic changes, as first outlined by Bryan in 1911 and later refined with modern notation by Hopkin in 1970, is particularly effective for classical aircraft experiencing small perturbations.

The approach assumes that the aerodynamic force and moment terms in the equations of motion depend solely on the disturbed motion variables and their derivatives. Mathematically, this is represented by a series of Taylor series expansions, with each series involving one motion variable or its derivative. The motion variables in question are the linear velocities (u, v, w) and the angular rates (p, q, r) .

For example, the axial force equation's aerodynamic term, (X_a) , can be expressed as a function of these variables and their derivatives. The equation is simplified by considering only the first term in each series, as the motion variables are small and higher-order terms are typically insignificant. The only higher-order derivative terms that are commonly significant involve (\dot{w}) .

$$X_a = X_{ae} + \frac{\partial X}{\partial u}u + \frac{\partial X}{\partial v}v + \frac{\partial X}{\partial w}w + \frac{\partial X}{\partial p}p + \frac{\partial X}{\partial q}q + \frac{\partial X}{\partial r}r + \frac{\partial X}{\partial \dot{w}}\dot{w} \quad (2.11)$$

Equation 2.12 may also be simplified as :

$$X_a = X_a + \dot{x}_u u + \dot{x}_v v + \dot{x}_w w + \dot{x}_p p + \dot{x}_q q + \dot{x}_r r + \dot{x}_{\dot{w}} \dot{w} \quad (2.12)$$

2.3.5 Aerodynamics Control Terms

The aerodynamic control terms describe the forces and moments generated by the deflections of the primary aerodynamic controls, which include the elevator, ailerons, and rudder. These control surfaces alter the airflow around the aircraft, thereby changing the aerodynamic forces and moments acting on it. The effects of these control deflections are quantified in terms of aerodynamic control derivatives.

The aerodynamic control derivatives are partial derivatives that represent the change in aerodynamic forces and moments with respect to changes in control surface deflections. These derivatives are evaluated at the prevailing trim condition, which is the state of the aircraft when the control surfaces are not deflected.

The pitching moment due to aerodynamic controls, for example, can be expressed as follows:

$$M_c = \left(\frac{\partial M}{\partial \xi} \right) \xi + \left(\frac{\partial M}{\partial \eta} \right) \eta + \left(\frac{\partial M}{\partial \zeta} \right) \zeta \quad (2.13)$$

In this equation:

- (M_c) is the pitching moment due to aerodynamic controls.
- (ξ, η, ζ) represent the aileron angle, elevator angle, and rudder angle, respectively.
- $(\frac{\partial M}{\partial \xi}, \frac{\partial M}{\partial \eta}, \frac{\partial M}{\partial \zeta})$ are the aerodynamic control derivatives for the aileron, elevator, and rudder, respectively.

These control angles are measured relative to their trim settings, denoted as (ξ_e, η_e, ζ_e) . The shorthand notation used in the document simplifies the expression of the pitching moment due to aerodynamic controls to:

$$M_c = \overset{\circ}{M}_\xi \xi + \overset{\circ}{M}_\eta \eta + \overset{\circ}{M}_\zeta \zeta \quad (2.14)$$

2.3.6 Power Terms

The power terms in the equations of motion relate to the thrust produced by the aircraft's engines, which is controlled by the throttle lever angle, denoted as ε . When the throttle lever is moved, it results in a change in thrust, which in turn affects the forces and moments acting on the airplane. These effects are conveniently described using engine thrust derivatives, which are mathematical representations of how forces and moments change with respect to changes in thrust. An example provided is the normal force due to thrust, which is expressed in shorthand notation as :

$$Z_p = \dot{Z}_\tau \tau \quad (2.15)$$

2.3.7 EOM for Small Perturbations

In order to complete the creation of the linearized equations of motion, we just need to replace the proper formulations for the aerodynamic, gravitational, aerodynamic control, and thrust terms into equations (2.9).

$$\begin{aligned}
m(\dot{u} + qW_e) &= X_{a_e} + \dot{X}_u u + \dot{X}_v v + \dot{X}_w w + \dot{X}_p p + \dot{X}_q q + \dot{X}_r r + \dot{X}_{\dot{w}} \dot{w} \\
&\quad - mg \sin \theta_c - mg \theta \cos \theta_c + \dot{X}_\xi \xi + \dot{X}_\eta \eta + \dot{X}_\zeta \zeta + \dot{\tau} \tau \\
m(\dot{v} - pW_e + rU_e) &= Y_{a_e} + \dot{Y}_u u + \dot{Y}_v v + \dot{Y}_w w + \dot{Y}_p p + \dot{Y}_q q + \dot{Y}_r r + \dot{Y}_{\dot{w}} \dot{w} \\
&\quad + mg \psi \sin \theta_e + mg \phi \cos \theta_e + \dot{Y}_\xi \xi + \dot{Y}_\eta \eta + \dot{Y}_\zeta \zeta + \dot{Y}_\tau \tau \\
m(\dot{w} - qU_e) &= Z_{a_e} + \dot{Z}_u u + \dot{Z}_v v + \dot{Z}_w w + \dot{Z}_p p + \dot{Z}_q q + \dot{Z}_r r + \dot{Z}_{\dot{w}} \dot{w} \\
&\quad + mg \cos \theta_c - mg \theta \sin \theta_c + \dot{Z}_\xi \xi + \dot{Z}_\eta \eta + \dot{Z}_\zeta \zeta + \dot{\tau} \tau \\
I_x \dot{p} - I_{xz} \dot{r} &= L_{a_e} + \dot{L}_u u + \dot{L}_v v + \dot{L}_w w + \dot{L}_p p + \dot{L}_q q + \dot{L}_r r \\
&\quad + \dot{L}_{\dot{w}} \dot{w} + \dot{L}_\xi \xi + \dot{L}_\eta \eta + \dot{L}_\zeta \zeta + \dot{L}_\tau \tau \\
I_y \dot{q} &= M_{a_e} + \dot{M}_u u + \dot{M}_v v + \dot{M}_w w + \dot{M}_p p + \dot{M}_q q + \dot{M}_r r \\
&\quad + \dot{M}_{\dot{w}} \dot{w} + \dot{M}_\xi \xi + \dot{M}_\eta \eta + \dot{M}_\zeta \zeta + \dot{M}_\tau \tau \\
I_z \dot{r} - I_{xz} \dot{p} &= N_{a_e} + \dot{N}_u u + \dot{N}_v v + \dot{N}_w w + \dot{N}_p p + \dot{N}_q q + \dot{N}_r r \\
&\quad + \dot{N}_{\dot{w}} \dot{w} + \dot{N}_\xi \xi + \dot{N}_\eta \eta + \dot{N}_\zeta \zeta + \dot{N}_\tau \tau
\end{aligned} \tag{2.16}$$

Since all perturbation variables and their derivatives are zero by definition in the stable trimmed flying condition, the steady state equations (2.16) reduce to:

$$\begin{aligned}
X_{a_e} &= mg \sin \theta_e \\
Y_{a_e} &= 0 \\
Z_{a_e} &= -mg \cos \theta_e \\
L_{a_e} &= 0 \\
M_{a_e} &= 0 \\
N_{a_e} &= 0
\end{aligned} \tag{2.17}$$

Equations (2.17) indicate the constant trim terms that may be replaced in equations (2.16). After rearrangement, they can be expressed as:

$$\begin{aligned}
& m\dot{u} - \dot{X}_u u - \dot{X}_v v - \dot{X}_{\dot{w}} \dot{w} - \dot{X}_w w \\
& - \dot{X}_p p - \left(\dot{X}_q - mW_e \right) q - \dot{X}_r r + mg\theta \cos \theta_e = \dot{X}_\xi \xi + \dot{X}_\eta \eta + \dot{X}_\zeta \zeta + \dot{X}_\tau \tau \\
& - \dot{Y}_u u + m\dot{v} - \dot{Y}_v v - \dot{Y}_{\dot{w}} \dot{w} - \dot{Y}_w w - \left(\dot{Y}_p + mW_e \right) p \\
& - \dot{Y}_q q - \left(\dot{Y}_r - mU_e \right) r - mg\phi \cos \theta_e - mg\psi \sin \theta_e = \dot{Y}_\xi \xi + \dot{Y}_\eta \eta + \dot{Y}_\zeta \zeta + \dot{Y}_\tau \tau \\
& - \dot{Z}_u u - \dot{Z}_v v + \left(m - \dot{Z}_{\dot{w}} \right) \dot{w} - \dot{Z}_w w \\
& - \dot{Z}_p p - \left(\dot{Z}_q + mU_e \right) q - \dot{Z}_r r + mg\theta \sin \theta_e = \dot{Z}_\xi \xi + \dot{Z}_\eta \eta + \dot{Z}_\zeta \zeta + \dot{Z}_\tau \tau \\
& - \dot{L}_u u - \dot{L}_v v - \dot{L}_{\dot{w}} \dot{w} - \dot{L}_w w \\
& + I_x \dot{p} - \dot{L}_p p - \dot{L}_q q - I_{xz} \dot{r} - \dot{L}_r r = \dot{L}_\xi \xi + \dot{L}_\eta \eta + \dot{L}_\zeta \zeta + \dot{L}_\tau \tau \\
& - \dot{M}_u u - \dot{M}_v v - \dot{M}_{\dot{w}} \dot{w} \\
& - \dot{M}_w w - \dot{M}_p p + I_y \dot{q} - \dot{M}_q q - \dot{M}_r r = \dot{M}_\xi \xi + \dot{M}_\eta \eta + \dot{M}_\zeta \zeta + \dot{M}_\tau \tau \\
& - \dot{N}_u u - \dot{N}_v v - \dot{N}_{\dot{w}} \dot{w} - \dot{N}_w w \\
& - I_{xz} \dot{p} - \dot{N}_p p - \dot{N}_q q + I_z \dot{r} - \dot{N}_r r = \dot{N}_\xi \xi + \dot{N}_\eta \eta + \dot{N}_\zeta \zeta + \dot{N}_\tau \tau
\end{aligned} \tag{2.18}$$

2.4 Aircraft Stability

According to [10] the definition of aircraft stability motions limits to only small perturbations which its model is linearized. it is stated that "A system which is initially in a state of static equilibrium is said to be stable if after a disturbance of finite amplitude and duration the response ultimately becomes vanishingly small" [10] as a definition of stability of a linear system. In other words, Stability of an aircraft is assessed by the condition of motion aircraft after having some perturbation, whether it returns to its initial position (trim condition) or not. Trim state happens when the aircraft is flying in a straight line at a constant speed

and all forces acting on the aircraft are in balance. The stability requirements based on FAR 23 for light aircraft in short:

- The aircraft non aerobatics must have static longitudinal, lateral, and directional stability in normal operations.
- Stable in dynamic short period and Dutch roll.
- Stable control force feedback throughout the operating envelope.
- No aircraft may exhibit divergent longitudinal stability characteristic so unstable.

and for UAV based on Stanag 4671 in short:

- The UAV, augmented by the FCS including all degraded modes, must be longitudinally, directionally and laterally stable in any condition normally encountered in service, at any combination of weight and centre of gravity for which certification is requested.
- Transient response in all axes during transition between different flight conditions and flight modes must be smooth, convergent, and exhibit damping characteristics with minimal overshoot of the intended flight path.
- In addition to data obtained by computation or modelling, stability analysis must be supported by the results of relevant flight tests.
- Demonstration of static and dynamic stability are not applicable.

The main difference between these 2 regulations is that Stanag 4671 does not require the UAV to be naturally stable but rather stable by using the augmented system by FCS. In Stanag 4671, it is also stated that all the motion modes must exhibit smooth, convergent, and damping characteristics after being augmented by FCS.

2.4.1 Modes of Aircraft Motion

Aircraft motion on 3D space can be classified into 2 modes, namely:

- Longitudinal Mode
Aircraft moves along X_b , Z_b axis and rotates around Y_b axis.
- Lateral-Directional Mode
Aircraft moves inside 2 plane lateral plane (Y_b, Z_b) and directional plane(X_b, Y_b)

for more detailed information can be seen in Figure 2.4 and Figure 2.5

Parameters of motion in 3D space:

- Translation: X, Y, Z
- Rotations: ϕ, θ, ψ

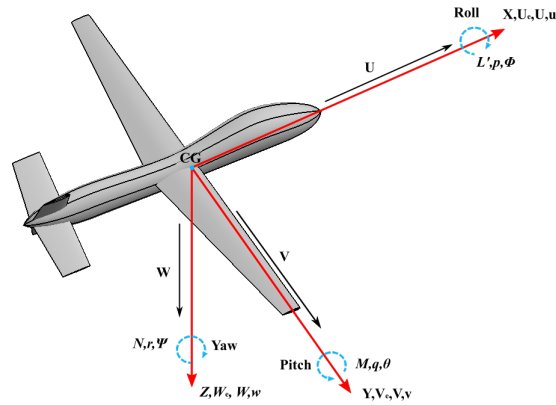


FIGURE 2.4: Aircraft Motion.

2.4.2 Reference Axes

Figure 2.5 indicates an airplane with relative wind on its side and the standard right-handed set of body-fixed reference frames. The body-fixed reference frame is frame B, which is connected to the vehicle's center of gravity and has its axes aligned with the fuselage reference line. Two reference frames are added, both of which are tied to the vehicle's center of gravity (cg): the stability reference frame S, which is used to analyze the impact of deviations from steady-state flight, and the wind reference frame W. The angle of attack α and sideslip angle β are defined by a plane revolution around the body y axis followed by a plane rotation about the z axis, so that the final x axis is aligned with the relative wind. The first rotation produces the stability reference frame S, whereas the second produces the wind reference frame W. A positive α indicates a negative rotation

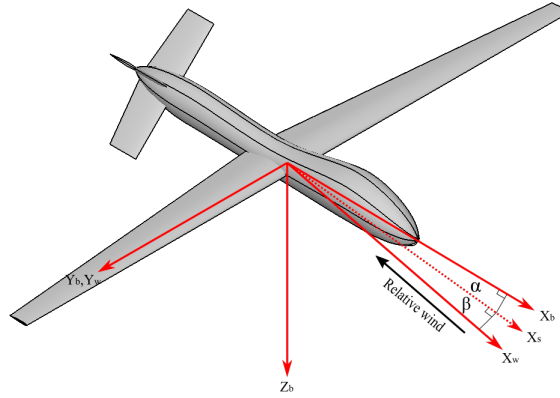


FIGURE 2.5: Reference axes.

along the y axis (positive in the illustration). If the rotation around the stability z axis was positive, the sideslip angle β is positive (is positive in the figure).

2.4.3 Static Stability and Dynamic Stability

Static stability refers to an aircraft's inherent ability to return to its original flight condition after a small disturbance. It is a measure of the aircraft's tendency to counteract deviations from its equilibrium state. When an aircraft is statically stable, any displacement from its trimmed condition will generate aerodynamic forces or moments that will restore it to its original position. The degree of static stability is influenced by factors such as the center of gravity (CG) position and the aerodynamic characteristics of the airframe. Static stability can be easily defined by the Figure 2.8. based on the Figure 2.8, there are 3 types of system. the first condition indicated the statically stable system, second, and third indicate statically unstable system and statically neutral system respectively. If a body tend to return to its initial position or equilibrium position under steady motion, it means that the body is statically stable. Statically stable system does not ensure the system is dynamically stable but dynamically stable system must be statically stable.

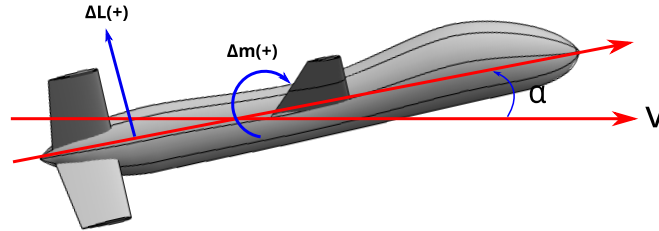


FIGURE 2.6: Longitudinal Stability.

Longitudinal static stability refers to the ability of an aircraft to maintain its equilibrium in the pitch axis during steady flight conditions. This is achieved when the aircraft's pitching moment, which is the force that causes an aircraft to pitch up or down, is stable and predictable. The change in pitching moment due to angle of attack is a key factor in determining longitudinal static stability.

For an aircraft to be longitudinally stable, it must have a negative value of Cm_{α} ($CM_{\alpha} < 0$). This means that when there is a positive disturbance, such as an increase in angle of attack, the aircraft should naturally produce a negative moment that opposes the disturbance and helps to restore the aircraft to its original equilibrium position [11]. In addition, a positive value of Cl_{α} ($CL_{\alpha} > 0$) can also indicate longitudinal static stability for an aircraft with the center of gravity in front of the aircraft's aerodynamic center [12].

Lateral-directional static stability, on the other hand, refers to the ability of an aircraft to maintain its equilibrium in the roll and yaw axes during steady flight conditions. This is achieved when the aircraft's rolling and yawing moments are stable and predictable. The main conditions for lateral-directional static stability are $Cl_{\beta} < 0$ and $Cn_{\beta} > 0$ [12].

When there is a positive beta (β) disturbance, such as a sideways gust of wind, the aircraft should naturally produce a negative roll moment L (rolling to

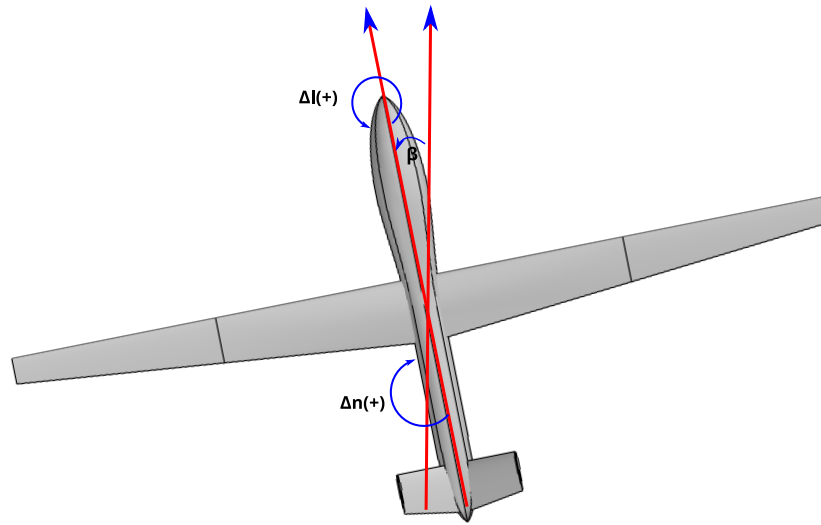


FIGURE 2.7: Lateral-Directional Stability.

the left) and a positive yaw moment N (yawing to the right) that opposes the disturbance and helps to restore the aircraft to its original equilibrium position [11]. Additionally, a negative value of C_y (side force coefficient) can also indicate aircraft lateral-directional static stability.

Dynamic stability, on the other hand, concerns the aircraft's behavior over time after a disturbance. It describes how the aircraft's motion evolves, whether it dampens out to return to equilibrium or continues to diverge. An aircraft can be statically stable but dynamically unstable if, after an initial disturbance, it exhibits oscillations that increase in amplitude over time (see Fig. 2.9).

The relationship between static and dynamic stability is complex and interdependent. Both types of stability are essential for an aircraft to be considered safe and controllable. The degree of stability — shown by Fig. 2.10 — affects the aircraft's responsiveness to control inputs and its resistance to disturbances. A highly stable aircraft may require more significant control inputs to maneuver, while an aircraft with too little stability may be overly responsive, leading to potential over-control by the pilot.

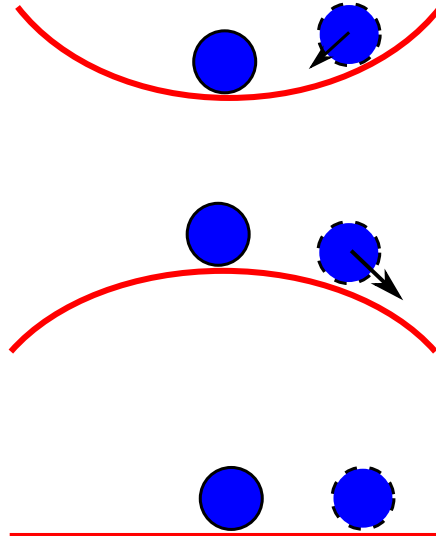


FIGURE 2.8: Illustration of static stability reprinted from [13].

2.4.4 Characteristic Equations

The characteristic equation is a fundamental concept in the analysis of aircraft stability. It is derived from the denominator of the aircraft response transfer functions, and its roots, known as the poles, determine the stability modes of the airplane. When the characteristic polynomial is set to zero, we obtain the characteristic equation.

For aircraft where the motion can be considered decoupled, two separate fourth-order characteristic equations emerge: one for longitudinal symmetric motion and another for lateral-directional asymmetric motion. However, for more complex aircraft like helicopters, or those with significant stability augmentation from flight control systems, the characteristic equation can be of much higher

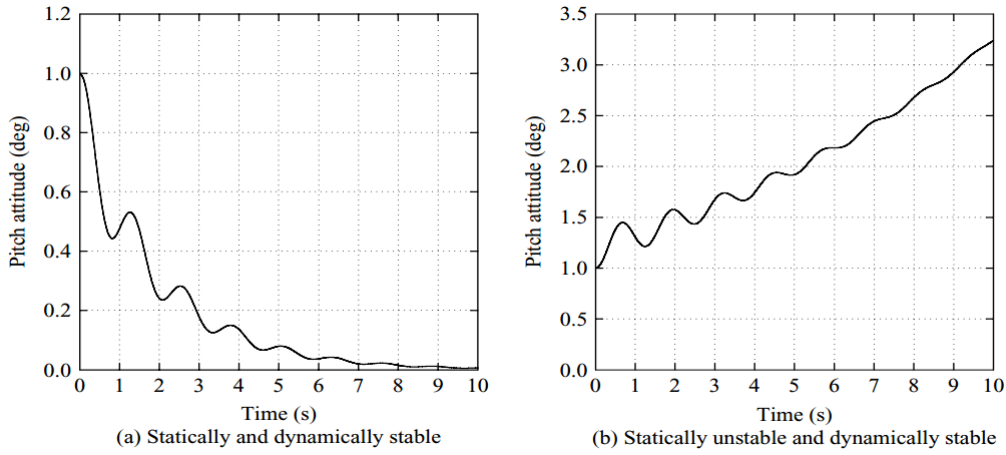


FIGURE 2.9: Stability Comparison reprinted from [10].

order, such as eighth order or even up to 30th order for advanced combat aircraft. These high-order equations can be challenging to interpret due to the increased complexity.

The general form of the characteristic equation for a system of order (n) is given by:

$$\Delta(s) = a_n s^n + a_{n-1} s^{n-1} + a_{n-2} s^{n-2} + \dots + a_1 s + a_0 = 0 \quad (2.19)$$

The stability of the system is determined by the nature of the roots of this equation. If all coefficients (a_n, a_{n-1}, \dots, a_0) are real, the roots can be real or complex pairs. The roots can be expressed as:

- Single real roots, for example, ($s = -\sigma_1$) with the time solution ($k_1 e^{-\sigma_1 t}$).
- Complex pairs of roots, for example, ($s = -\sigma_2 \pm j\gamma_2$) with the time solution ($k_2 e^{-\sigma_2 t} \sin(\gamma_2 t + \phi_2)$), or equivalently ($s^2 + 2\sigma_2 s + (\sigma_2^2 + \gamma_2^2) = 0$).

A system is considered stable if all roots have negative real parts, meaning any disturbance will decay over time. If any root has a positive real part, the system is unstable, and disturbances will grow. A system with roots having zero real parts is neutrally stable, indicating that disturbances neither grow nor decay.

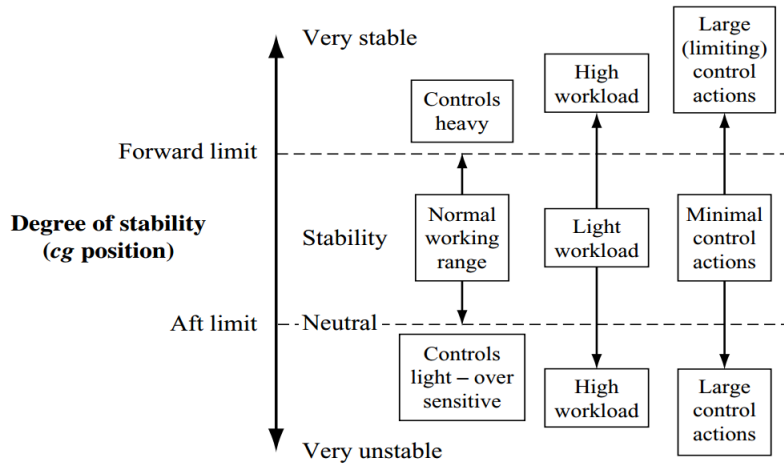


FIGURE 2.10: Illustration of Degree of Stability reprinted from [10].

2.4.5 Root Mapping on the S-Plane

The s-plane is a graphical representation where the horizontal axis represents the real part of the roots (or poles) and the vertical axis represents the imaginary part. Stability of the system is determined by the location of the poles on this plane. For a system to be stable, all poles must lie on the left half of the s-plane, which corresponds to negative real parts.

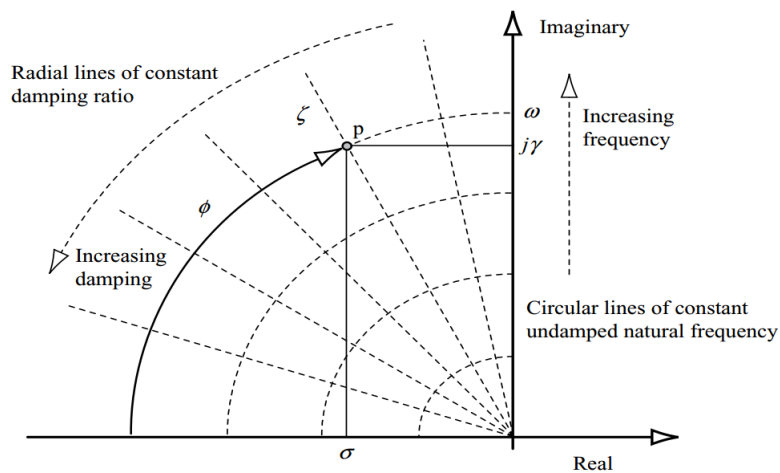


FIGURE 2.11: Splan reprinted from [10].

The complex roots 2.11 are plotted at a point labeled 'p' in the upper half of

the s-plane. Since the roots of the characteristic equation are complex conjugates, only the upper half of the s-plane is shown, as the lower half is a mirror image across the real axis.

The figure demonstrates that lines of constant undamped natural frequency (ω) are circles concentric with the origin, assuming both axes have the same scale. If the scales are different, these lines become ellipses. The magnitude of the line joining the origin to the point 'p' represents the undamped natural frequency of the system.

Radial lines through the origin represent lines of constant damping ratio (ζ). The imaginary axis (where the real part is zero) is the line of zero damping, and the real axis (where the imaginary part is zero) is the line of critical damping, where the damping ratio is unity, and the roots become real.

The upper left quadrant of the s-plane contains the stable region where the damping ratio is between 0 and 1. Roots in this region indicate stable and well-damped dynamics. The closer the roots are to the left-hand side of the s-plane, the more stable the system is, as they have a larger negative real part, which corresponds to a faster decay of the transient response.

2.5 Previous Work

2.5.1 P.Panagioutou et al., 2016 [14]

This paper outlines the comprehensive aerodynamic design process for a Medium-Altitude Long-Endurance (MALE) Unmanned Aerial Vehicle (UAV), detailing both the conceptual and preliminary design phases. The study, conducted by researchers at the Aristotle University of Thessaloniki, Greece, is published in *Aerospace Science and Technology* Volume 50, 2016. It provides a structured approach to UAV design, integrating computational fluid dynamics (CFD) simulations with analytical calculations.

In the conceptual design phase, four teams utilized a common methodology to develop presizing tools and distinct UAV configurations based on uniform mission requirements. These different concepts were evaluated and merged into a singular design concept, which laid the foundation for the preliminary design phase.

The preliminary design emphasized detailed aerodynamic aspects, including the designs of the fuselage, wings, empennage, and winglets, as well as the cooling study for engine inlets. The document presents analytical methods employed at each stage, supported by detailed CFD computations. The final UAV concept, including geometric, aerodynamic, stability, and performance parameters, is discussed and evaluated.

The results section reports that the final design exceeds initial endurance requirements by over 30%, albeit at a slightly compromised maximum velocity due to budget constraints. The UAV is deemed inherently stable with an endurance of over 10 hours, a 6.4-meter wingspan, and a 25 hp two-stroke engine. The study concludes that the design process effectively integrated CFD simulations with analytical methods, producing a UAV design that meets the set requirements and can serve as a template for future UAV projects.

2.5.2 Zdobyslaw Goraj, 2004 [15]

The paper details the proceedings of the AIAA 3rd "Unmanned Unlimited" Technical Conference, with a specific focus on the PW-125 MALE (Medium Altitude Long Endurance) UAV (Unmanned Aerial Vehicle) design project developed at Warsaw University of Technology. The presentation by Zdobyslaw Goraj showcases two conceptual UAV design projects emphasizing suitability for intended missions, leveraging international experience from past European Union-supported projects.

The initial project described is the PW-125, intended for light aircraft border surveillance missions, capitalizing on the design lineage of the PW-5 glider, with parts potentially producible using existing molds. The application is clear: to monitor and surveil the external borders of the European Union, with an underlying sentiment in Poland for the UAV to be domestically produced, albeit excluding components like sensors and control software.

The second project, PW-124, deviates significantly in purpose and design, targeting military applications with high maneuverability and reduced radar, infrared, and acoustic signature. While the university lacks the resources for full-scale development, it can contribute substantially up to in-flight testing using

scaled models. The PW-124 concept involves highly advanced design features, including a blended wing body and stealth characteristics, aimed at fulfilling military requirements for a low-cost, high-performance UAV. A

2.5.3 Ashish Karki et al., 2021 [16]

This academic paper is from the Proceedings of the 10th IOE Graduate Conference, detailing the conceptual design and stability analysis of a fixed-wing Unmanned Aerial System (UAS) intended for aerial experiments. The research addresses the limitations of multirotor drones, such as limited endurance and payload capacity, by proposing a fixed-wing UAS that can sustain longer flights with higher efficiency.

In the introduction, the authors outline the expansive use of UAS in various civil applications, highlighting their operational flexibility and cost-effectiveness. They note the limited endurance of multirotor drones and the potential of fixed-wing alternatives to overcome these limitations, despite challenges in control and stability design. The conceptual design process involves estimating takeoff weight, conducting constraint analysis, selecting configurations for the wing and propulsion system, and evaluating the UAS's performance.

The document describes the estimation of the UAS's takeoff weight by calculating the weights of subsystems, such as structure, actuators, avionics, and payload. Constraint analysis is used to determine feasible design points by considering requirements for stall speed, climb rate, takeoff run, and cruise performance. The wing and tail configurations are selected based on operational, manufacturing, and stability requirements, with a V-tail configuration being the preferred choice for the tail, and a straight taper wing being chosen for its design simplicity. The propulsion system is sized based on the maximum power required during takeoff, with an electric brushless motor and propeller recommended.

Stability analysis is divided into static and dynamic considerations. Static stability examines the UAS's tendency to return to equilibrium after a disturbance, while dynamic stability looks at the motion over time following such a disturbance. The UAS is modeled in XFLR5, a low-fidelity analysis tool, to assess stability in longitudinal, lateral, and directional axes. The results indicate that

the UAS possesses adequate static margin for longitudinal stability and is directionally stable, but compromises lateral stability for simplicity in manufacturing and operation. Dynamic stability analysis identifies various modes of oscillation, including short-period, phugoid, dutch-roll, roll subsidence, and spiral modes, concluding that all modes except the spiral mode are convergent, implying overall dynamic stability.

In conclusion, the paper asserts the proposed UAS design is a viable alternative to multirotor drones for applications requiring longer endurance and larger payload capacities. Although the lateral stability is a trade-off for simplicity, the UAS is stable in other aspects and can be managed manually or with flight control systems. The authors suggest future work to include flight simulation and experimental testing to validate the numerical results.

2.5.4 A. Septiyana et al., 2020 [17]

This paper is a comprehensive report from the AIP Conference Proceedings detailing a 2020 study on the aerodynamic analysis of the LSU 05-NG unmanned aircraft using the Vortex Lattice Method (VLM). The research was conducted by A. Septiyana and colleagues from the Aeronautics Technology Center, National Institute of Aeronautics and Space (LAPAN), Indonesia. The study aimed to utilize VLM with XFLR5 software to assess key aerodynamic parameters such as lift coefficient (CL), drag coefficient (CD), moment coefficient (CM), and the lift-to-drag ratio (L/D). The study found that VLM is effective in predicting the lift coefficient but less so for the drag coefficient due to the assumption of inviscid flow, which does not account for fluid viscosity. Consequently, the L/D analysis using VLM displayed higher values compared to simulations with CFX, a computational fluid dynamics (CFD) software, because VLM does not model the effects of air viscosity or flow separation.

Results and discussions reveal that while VLM can predict lift coefficients well, it falls short in accurately determining drag coefficients due to its inviscid flow assumption. This affects the analysis of L/D, where VLM results in optimistic outcomes compared to CFX simulations. The document also highlights the aircraft's stability, indicated by negative pitching moments. It concludes that VLM

is a useful method for aerodynamic analysis but requires further development to provide a more accurate picture of aerodynamic characteristics, especially concerning drag and efficiency.

CHAPTER 3

RESEARCH METHODOLOGY

3.1 Conceptual Design Process Flowchart

In Chapter 3 the methodology of this thesis will be discussed. Figure 3.1 represents the steps taken throughout the entire process of making this thesis.

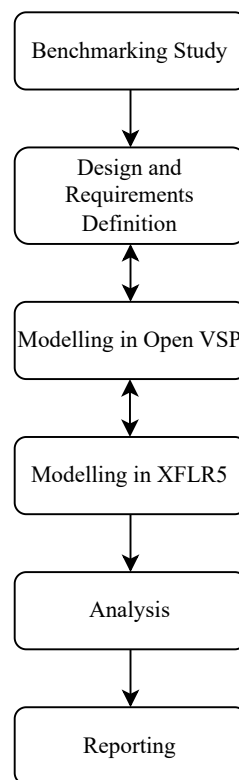


FIGURE 3.1: Research Methodology

3.2 Benchmarking Study

The benchmarking investigation began during the early phases of the conceptual design process. The primary purpose was to assess and compare the performance and characteristics of different Medium Altitude Long Endurance (MALE) Unmanned Aerial Vehicles (UAVs) that are now operating or in development. This broad analysis comprised a sample of 22 different UAV types. Critical aspects such as performance measurements, aerodynamic properties, and configuration were extensively examined to ensure their capability and acceptance.

The study included a detailed assessment of these factors to discover UAVs that satisfied our demanding criteria for conceptual design of a MALE UAV. Following a thorough assessment, the MQ-1 Predator and Elbit Hermes 900 Starliner were chosen as the principal models for reference. These platforms were chosen using a number of criteria. The MQ-1 Predator has a proven track record of performance and reliability, making it the industry standard for MALE UAVs, whereas the Elbit Hermes 900 Starliner is STANAG 4671 compliant. Compliance with STANAG 4671 is especially important because it indicates that the UAV meets the requirements for unrestricted operation in NATO member countries' airspace, ensuring broad operational clearance and interoperability with friendly forces.

The selection of these two UAVs offers the basis for the development of our hypothetical MALE UAV. By adhering to the MQ-1 Predator's proven performance criteria and adding the Elbit Hermes 900 Starliner's sophisticated compliance features, we want to produce a UAV that not only meets but exceeds the operational standards and expectations of future aerial operations. For detailed information of this benchmarking study table can be seen in the Appendix [.2](#).

3.3 Mission Profile and Design Requirements

The mission profile is based on the user's requirements. As a result, different configurations require the creation of different mission profiles. The mission profile for this conceptual design was established after conducting a market benchmarking analysis on MALE UAVs. Two UAVs were chosen as a reference from the

benchmarking study, which is Hermes Starliner and MQ-1. Figure 3.2 shows the design requirements and mission profile. The design requirements and mission profile were reproduced from [18] with 1.1x performance improvement, where the author got the informations based on modified version of MQ-9 in the public domain. Furthermore, various mission types were conceptualized and divided into three major categories: combat, intelligence, surveillance, reconnaissance (ISR), and search and rescue (SAR). Each category has unique payload design criteria reflecting the various operational objectives and tactical demands of these missions. The development of each configuration was guided by an examination of the available Mil-COTS (Military Commercial Off The Shelf) payload data, which, while limited, provided critical input for this stage of the design process. Detailed specifications for each payload component have been compiled and examined. This comprehensive data collection and analysis resulted in the predicted weight for each type of mission, which is an important aspect in the UAV's overall design and performance. The calculated payload weights for each mission type are listed below:

- Combat mission = 456.608 kg
- ISR mission = 183.408 kg
- SAR mission = 248.725 kg

3.3.1 Design Requirements

- Internal payload = 551.156lb (250 kg)
- MTOW = 3,417.165lb (1550kg)
- Endurance (clean) = 36hrs
- Max level speed = 120kt
- Cruising speed = 87kt
- Max rate of climb at S.L. = 1,200ft/min
- Max operating altitude = 30,000ft
- Max range = 1,350nm
- Field performance (take-off and landing) = \leq 5500ft (1676.4m)
- Limit load factors (as for GA Utility Aircraft) = +4.4 to -1.8

Mission Segment	Altitude (m)	Target Performance
1 Engine start, taxi, and take-off	0 to 15.24	726.948m
2 Climb	25.24 to 4572	100.11 km
3 Cruise Climb Ingress	7620	833.4 km
4 Loiter	7620	25 hour
5 Egress	7620 to 4572	833.4 km
6 Descent	4572 to Sea level	100.11 km
7 Landing, taxi, and shutdown	Sea level	726.948 m

3.3.2 Mission Profile and Target Performance

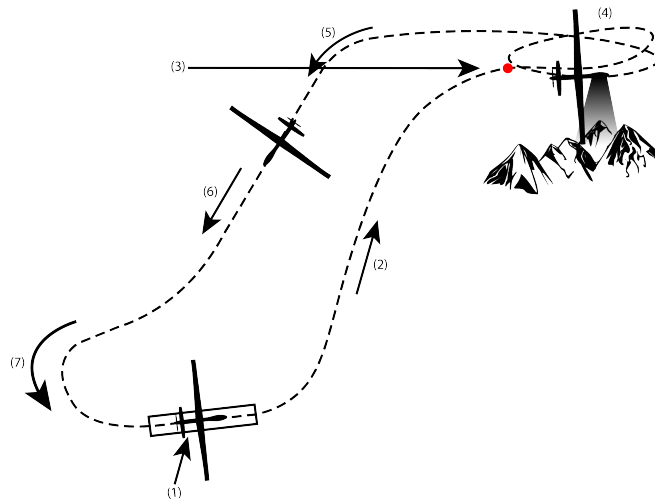


FIGURE 3.2: Mission Profile

3.4 Modelling in OpenVSP

3.4.1 Introduction to OpenVSP

OpenVSP (Open Vehicle Sketch Pad) is a parametric aircraft geometry tool where users can create a 3D model of an aircraft based primarily on engineering parameters. This tool was developed by J.R. Gloudemans and others for NASA since

the early 1990's and right now it is an open source tool, which means its source code is freely available for anyone to use and modify. OpenVSP is designed to create a three-dimensional representation of an aircraft using simple parameters such as wing span, chord length, fuselage length, etc. This allows for rapid exploration of aircraft designs and the generation of accurate geometries that can be used for further analysis. It is used by aerospace engineers, designers, educators, and students interested in aircraft design. It can be beneficial in the conceptual and preliminary stages of design. Users can define the major components of aircraft, such as wings, fuselage, empennage, nacelles, and other components. Each component can be modified through parameters. Changing a parameter updates the model in real-time, allowing for quick iterations. OpenVSP comes with a library of predefined components, which users can employ and customize for their specific design needs. While OpenVSP itself is primarily a geometry tool, it can integrate with other software for performing aerodynamic and structural analyses. Models created in OpenVSP can be exported to different formats compatible with Computational Fluid Dynamics (CFD) software, Finite Element Analysis (FEA) software, and CAD programs. In summary, OpenVSP serves as a valuable resource for those in the field of aerospace engineering, providing a robust platform for aircraft geometry creation and modification. Its open-source nature ensures that it is continuously improved upon and remains accessible to anyone interested in aircraft design [19].

3.4.2 Fuselage

The first step in modeling the geometric model in OpenVSP was by starting to design the fuselage part. There were 3 models of the fuselage were considered: These fuselage (Fig. 3.3) were designed by considering the size and volume of the internal parts of the UAV. From these 3 models the scoring matrix were used in order to choose which model offers best performance. The results of table matrix can be seen in Chapter 4.

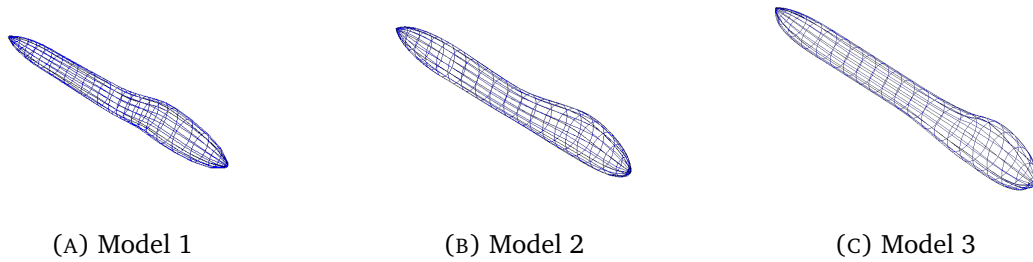


FIGURE 3.3: Fuselage Models

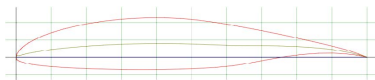


FIGURE 3.4:
NLF 0215

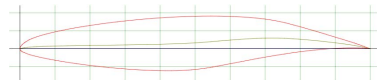


FIGURE 3.5:
NLF 0415

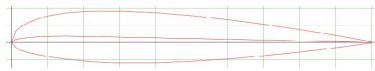


FIGURE 3.6:
NACA 23015

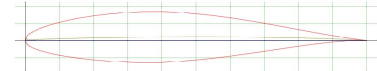


FIGURE 3.7:
NACA 64215

FIGURE 3.8: Airfoils Candidate

3.4.3 Airfoil

For the wing Airfoil, there were 4 candidates considered by using the airfoil matrix method. These airfoils can be seen in Figure 3.8. This grading method use values of range between 0 and 3, with 0 being the lowest point and 3 being the highest point. Finally, all the points added up to describe which airfoil had the best characteristics. The result of this grading method can be seen in the Chapter 4.

3.4.4 Wing Modelling

The wing modeling in OpenVSP is also quite similar to the fuselage modelling. OpenVSP has already prepared the predefined geometric shape of the wing. To create the geometric wing shape the first thing to do is setting the parameters of the wing on geometric menu, then set all of the parameters based on desired wing such as span, aspect ratio, sweep, airfoil and etc 3.13.

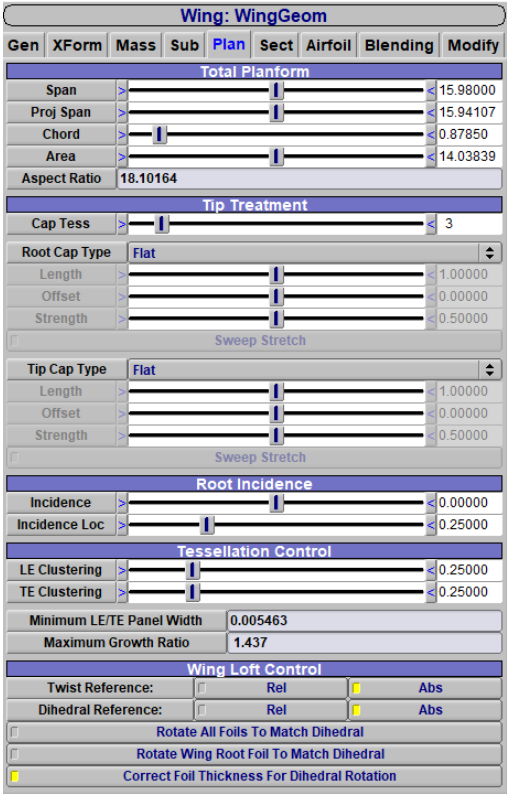


FIGURE 3.9:
Plan tab menu

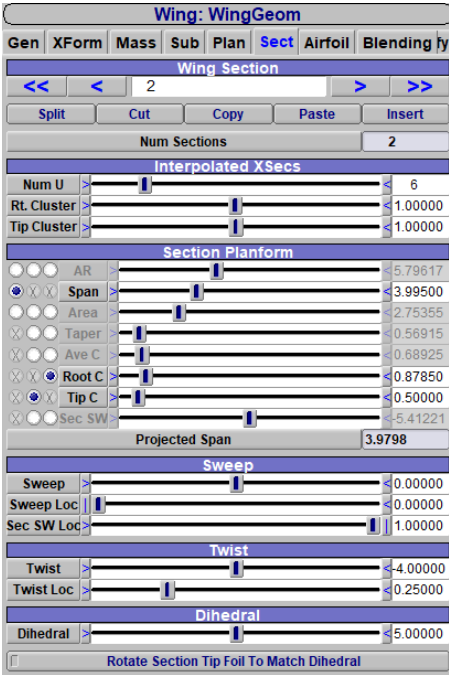


FIGURE 3.10:
Section tab
menu

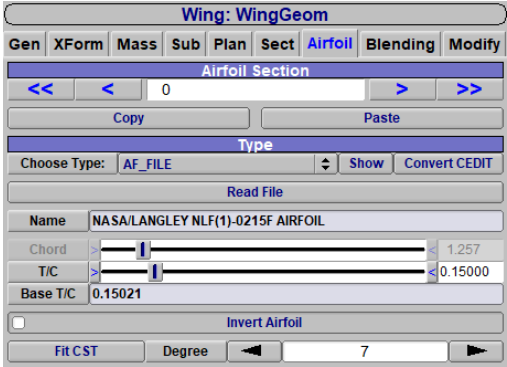


FIGURE 3.11:
Airfoil menu

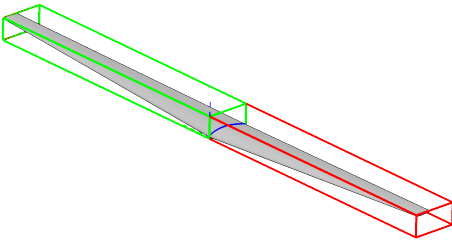


FIGURE 3.12:
Wing shape

FIGURE 3.13: Parameter setting

3.4.5 Tail Modelling

In OpenVSP, the process for modelling the tail is very similar to that of modelling the wing, with one key difference. The tail modelling is done with the setting planar on the XZ axis, which means that the tail will be mirrored on the other side of XZ plane. Once the tail has been modelled successfully, you need to assign a parametric value to it. This can be done in the wing geometric menu, as explained in the previous subchapter 3.4.4. Lastly, all of the geometrical shapes produced by Open VSP were then imported into CAD file format in order to create structure, such as a rib, spar, and so forth, by Mr. Akbar, as he is responsible for structural design.

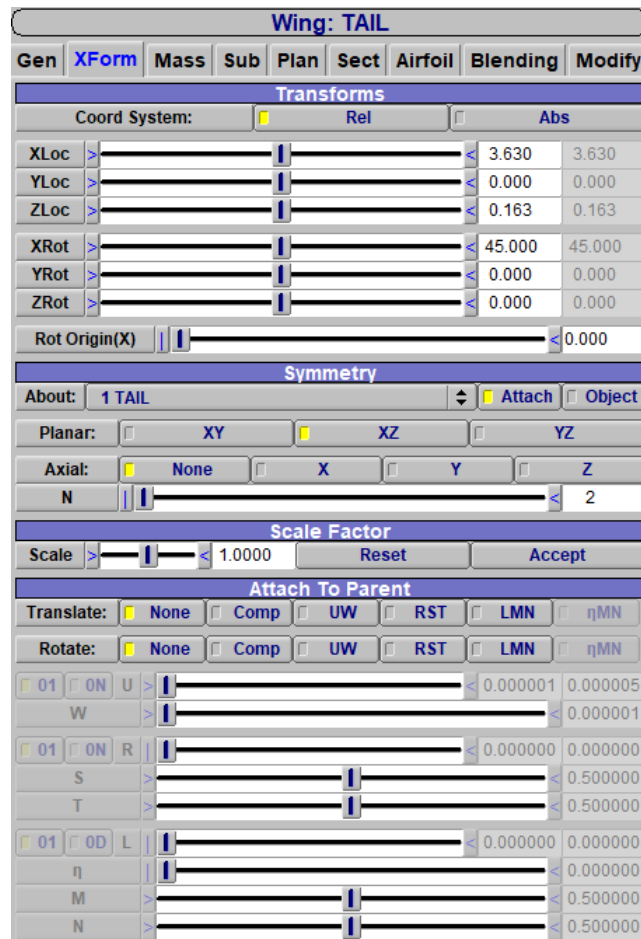


FIGURE 3.14: Tail Modelling

3.5 Modeling in XFLR5

3.5.1 Introduction to XFLR5

XFLR5 is an analysis tool for airfoils, wings, and planes operating at low Reynolds Numbers. It is particularly tailored for designing and analyzing subsonic isolated airfoils, though it has capabilities that extend to the analysis of wings and even full aircraft in certain conditions. XFLR5 is primarily used for the design and analysis of airfoils and their performance. It provides users with the ability to calculate the aerodynamic characteristics of airfoils and to analyze their behavior in two-dimensional or three-dimensional flows. It is a tool that sees frequent use in the hobbyist model aircraft community, as well as among students and educators in aerospace engineering for instructional purposes. Users can analyze the characteristics of airfoils such as lift, drag, and moment coefficients. It uses potential flow analysis along with boundary layer analysis for its calculations. Beyond airfoils, XFLR5 can perform analysis on 3D wings and planes using lifting line and vortex lattice methods. It is important to note that these methods assume inviscid, incompressible, and irrotational flow, which is a limitation for more complex analyses. XFLR5 allows for the computation of polars, which are plots of lift, drag, and moment coefficients against angle of attack. This is essential for understanding the aerodynamic performance of the airfoil or wing at various conditions. The software includes tools for modifying airfoil shapes and for designing wings. In conclusion, XFLR5 is a valuable software for those in the field of aerodynamics, particularly for applications involving low Reynolds Numbers. Its ease of use and the immediate visual feedback it provides make it an ideal educational tool, while its capabilities in airfoil and wing analysis are sufficient for many hobbyist and preliminary research applications.

3.5.2 Wing and Tail Shape Modelling

In order to create 3D wing and tail shape on XFLR5, first thing to do is to create the airfoil design in menu "Direct Foil Design" as shown in Figure 3.15. In this menu user can design the airfoil itself or import ".dat" airfoil file. For this thesis NACA 0012 as tail airfoil and NLF0215 as wing airfoil were chosen.

A CONCEPTUAL DESIGN OF FLEXIBLE MISSION MALE: AERODYNAMICS AND STABILITY

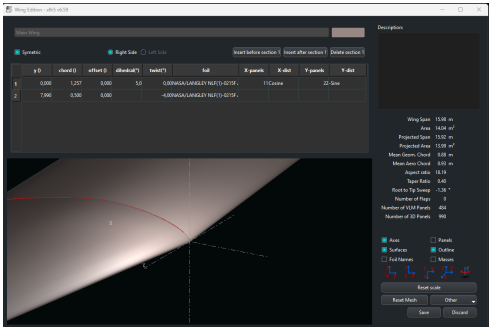


FIGURE 3.17:
Wing

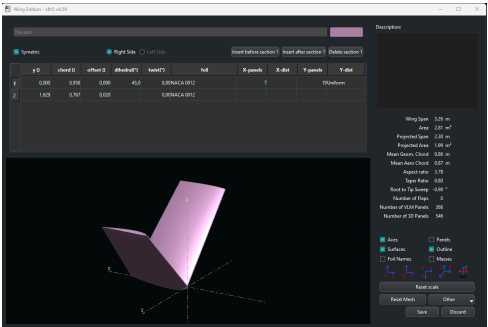


FIGURE 3.18:
Tail Upper

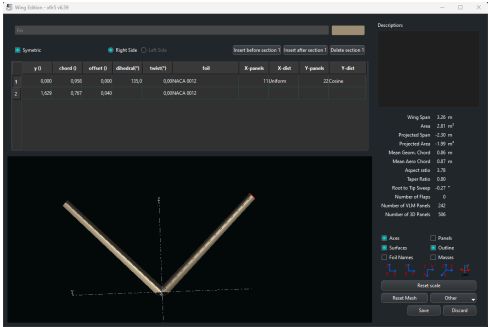


FIGURE 3.19:
Tail Lower

FIGURE 3.20: 3D Shape Wing and Tail

3.5.3 Mass Input

For the purpose of stability analysis, the mass must be input into the UAV air-frame. The mass for the structure based on the Figure 3.21 was divided into five parts, but the mass for the fuselage/body was not available because the XFLR5 manual said that it was not recommended to put fuselage shape into analysis; thus, mass input was not available. The reason for that is the implementation of the fuselage in XFLR5 is incomplete, so it will cause inaccurate results. For the subsystems additional point mass were used.

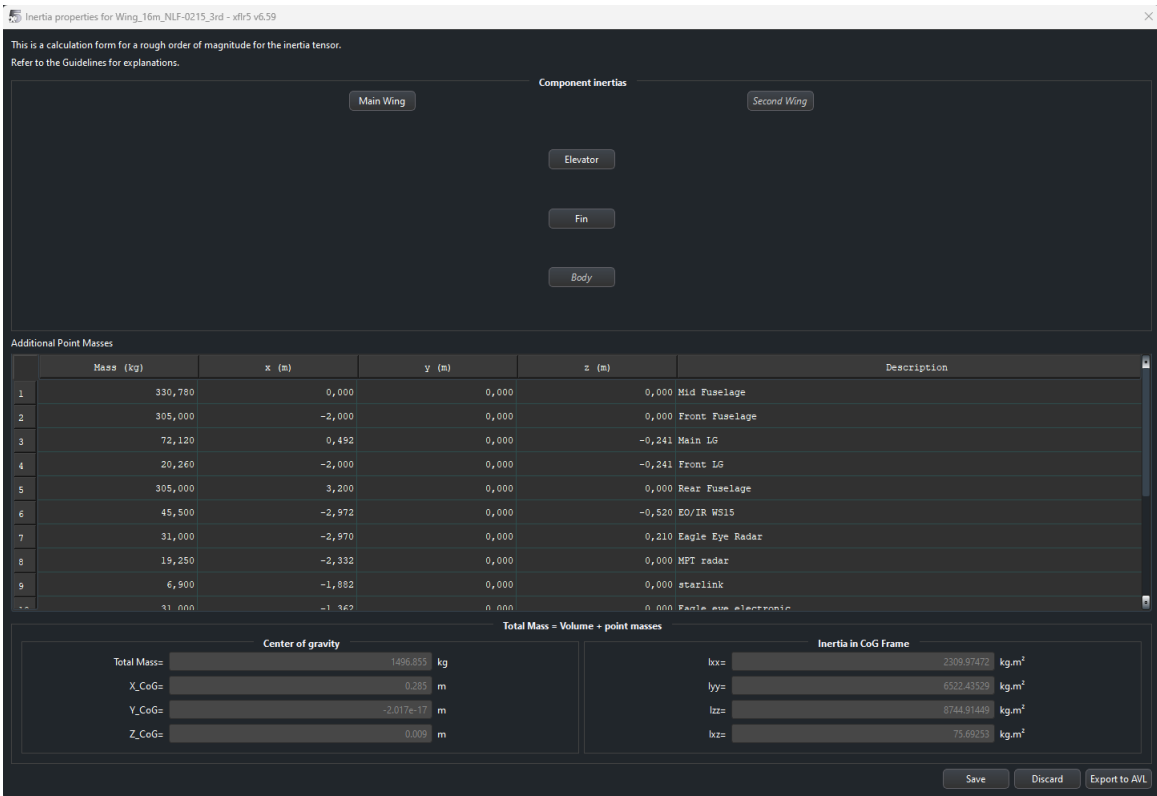


FIGURE 3.21: Mass Input

CHAPTER 4

RESULTS AND DISCUSSIONS

4.1 Weight Estimation

A comprehensive benchmarking study was undertaken on a total of 22 Medium Altitude Long Endurance (MALE) Unmanned Aerial Vehicles (UAVs). The objective of this study was to identify and select two reference MALE UAVs based on their performance and capabilities.

After the selection of these two reference UAVs, a detailed study was conducted to gather information about their respective payloads. This study involved collecting data from publicly available sources on the internet. The gathered data was then analyzed and compiled to estimate the weight of the payloads of these two reference UAVs. The results of this study, including the estimated weight of the payloads, can be found in a Table 4.1.

Furthermore, The weight estimations for the structure of the conceptual UAV was generated by my colleagues from its CAD drawings. The weight estimations for the structure can also be found in a separate Table 4.2. Lastly, based on the collected data of subsystems and payload by Mr. Akbar the MTOW of the maximum weight configuration is 1.497 kg.

4.2 Mass Input in XFLR5

In order to conduct a stability analysis through mass inputting, it is crucial to accurately define the location of each part. This can be achieved by referring to the CAD drawings of the UAV, which provides a comprehensive overview of each part's location. By carefully analyzing the CAD drawings, one can gain insight into the detailed location of each individual part. The detail location of each parts

	Mass (kg)	Descriptions
Avionics	17.002	Communication, FCC,MCC, and etc.
Imagery Payload	124.5	SAR Radar,EO/IR, Wide Imagery, and etc
Propulsion	101.244	Rotax 914F
Landing Gear	50	-
ISR Payload	38.5554	SIGINT
Combat Payload	613.2	Anti Submarine, Bomb Rack, and etc.
SAR Payload	65.3172	Life Support Raft

TABLE 4.1: Payload Weight

Material (AL2024)	
Section	Mass (kg)
Fuselage frame	1.187
Fuselage stringer	6.699
Wing Spar	14.211
Wing Rib	3.413
Empenage Spar	2.322
Empenage Rib	1.886
Fuselage skin	65.982
Wing skin	59.269
Empennage skin	41.678
Fuselage only	73.868
Wing only	76.893
Empennage only	45.886
Total frame	196.647

TABLE 4.2: Structural Weight

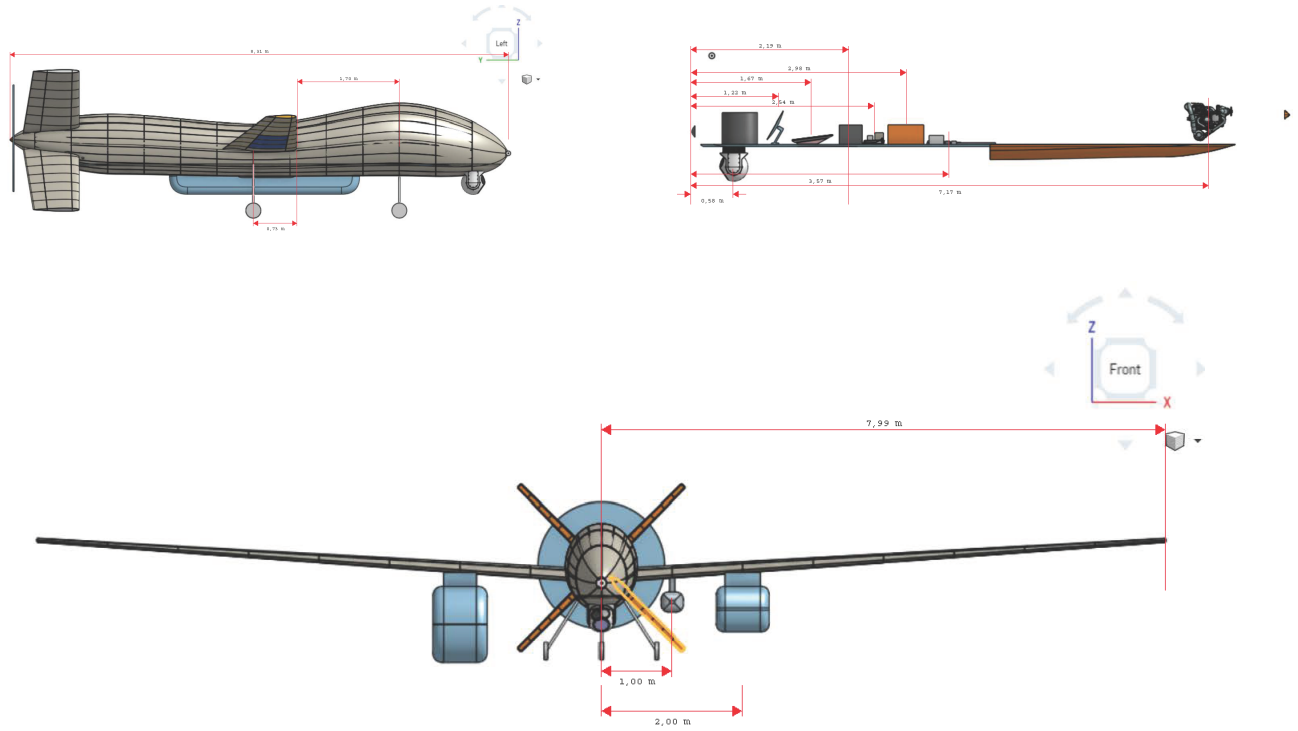


FIGURE 4.1: Parts Location

can be seen in Figure 4.1. Based on the CAD drawings, mass points are positioned as shown in the Figure 4.2. After all of the masses are inputted there were some small difference between cg location which calculated by XFLR5 and CAD design in onshape. The differences can be seen in Table 4.3. The calculated value of CG location differences can be caused by the point mass location in XFLR5 is not that accurate in comparison with onshape where the total geometrical shape masses are calculated rather than only a point in XFLR5. The additional mass of 3.698 kg could also be caused by the propeller mass, which was not inputted in XFLR5.

4.3 Aerodynamic Analysis

4.3.1 Configuration Selection

In the initial stages of the aircraft design, three different types of wing configurations - the joined wing, tandem wing, and conventional wing were considered.

	XFLR5	Onshape	Difference
XCG from fuselage's nose (m)	3.973	4.4227	0.4497
YCG (m)	0.079	0.076	0.003
ZCG (m)	0.115	0.12271	0.00771
Mass Total (Kg)	1493.644	1497.342	3.698

TABLE 4.3: Software calculation differences

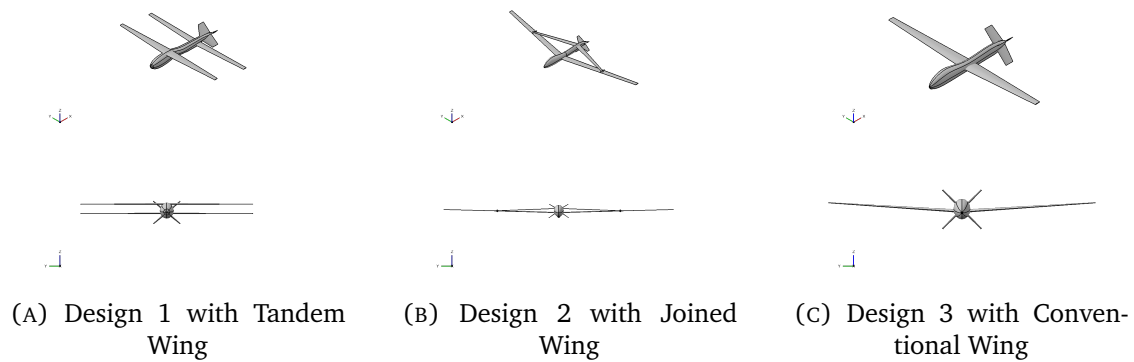


FIGURE 4.3: Three Wing Configuration

				*lowest = 3
Fuselage	C_{D0}	$Swet(m^2)$	$C_{D0}/Swet$	Score
Fuselage 1	0.00333	20.75	0.000160	2
Fuselage 2	0.00327	21.21	0.0001541	3
Fuselage 3	0.00319	20.64	0.0001546	1

TABLE 4.4: Scoring table fuselage

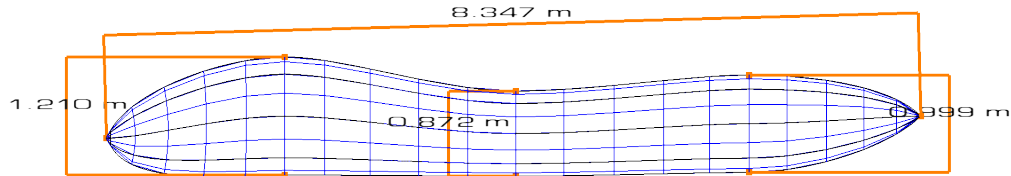


FIGURE 4.4: Fuselage Dimension

4.3.3 Airfoil

NACA 64215, NACA 23015, NLF 0215, and NLF0415 were chosen as potential candidates and the airfoil shape can be seen in Chapter 3 3.8. Figure 4.9 shows the aerodynamic performance of each airfoil each airfoil, and it was generated using XFOIL at $Re = 1 * 10^6$ & $Mach = 0.0$. In order to select the most appropriate airfoil based on parameters, a weighted scoring was used 4.5. NACA and NLF airfoils were chosen because of their characteristic, in which these airfoils were primarily designed to have favorable characteristics at high angles of attack and to provide good lift and drag performance over a wide range of conditions. NACA airfoils are generally characterized by a thick, cambered profile. On the other hand, NLF airfoils, as the name suggests, are designed to achieve natural laminar flow. The goal is to minimize boundary layer separation and maintain smooth, undisturbed airflow over the airfoil surface. NLF airfoils often have thinner profiles and employ various techniques to delay or prevent flow separation.

As a result, NLF0215 came out as the best among other airfoils. For the elevator and fin airfoil, NACA 0012 was selected as a preferable choice. This 12 % thickness airfoil offers several benefits to be used in elevators and fins. In terms of aerodynamic properties, It provides consistent aerodynamic characteristics for both positive and negative angles of attack, which is essential for control surfaces that need to deflect in both directions. At a 0° , it has zero lift, simplifying the

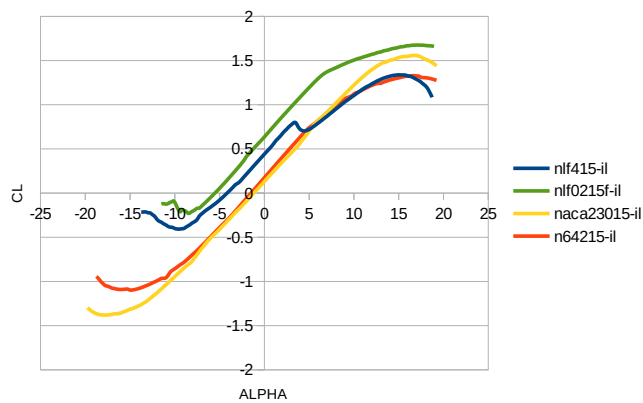


FIGURE 4.5:
CL VS Alpha

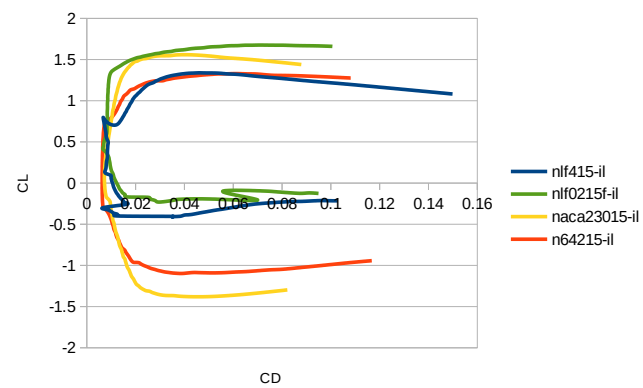


FIGURE 4.6:
CL VS Cd

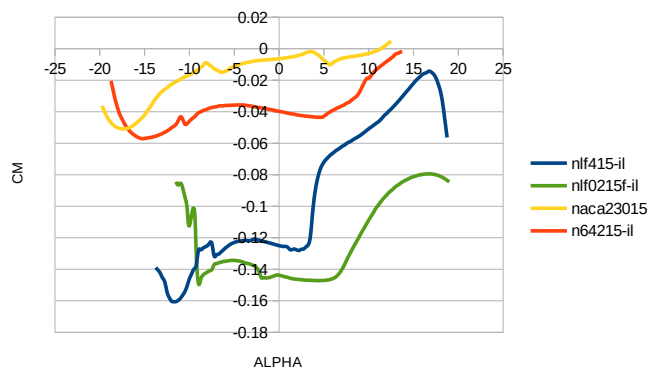


FIGURE 4.7:
Cm VS Alpha

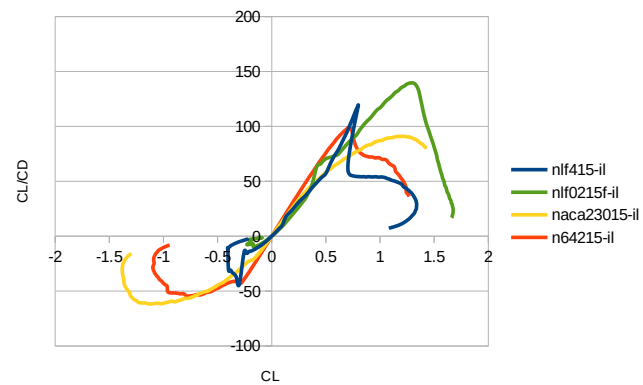


FIGURE 4.8:
CL/Cd VS CL

FIGURE 4.9: Airfoil Aerodynamic Characteristics

No	Parameter	NACA 23015	NACA 64215	NLF 0415	NLF 0215	Score				
1	Airfoil efficiency ratio (C_{lmax}/C_{dmin}) (high is the best)	216.662	227.2452	199.4933	253.5098	2.4	2.5	2.2	3	3
2	Thickness ratio (high is the best)	0.15	0.15	0.15	0.15	1	1	1	1	1
3	Re for data below	1×10^6	1×10^6	1×10^6	1×10^6					
5	AOA for $C_l = 0$	-1.25	-3	-4.25	-5.5					
6	C_{lmax} (highest is best)	1.5578	1.4271	1.3386	1.6757	2.5	2.3	2	3	3
7	AOA of C_{lmax} (highest is best)	16.5	17.5	15	17	2.8	3	2.6	2.9	2.9
8	Stall Characteristic (A, B, or C) (A is best)	C	B	C	A	1	2	1	3	3
9	C_{dmin} (lowest is best)	0.0072	0.0063	0.0067	0.0066	2.6	3	2.8	2.9	2.9
10	Sensitive to surface quality? (N is better)	N	Y	Y	Y	1	0	0	0	0
11	(C_l/C_d)max (highest is best)	90.95	120.62	118.36	139.71	2	2.6	2.5	3	3
12	C_l of (C_l/C_d)max (low C_l is best)	1.2224	0.718	0.7942	1.2965	2	3	2.6	1	1
13	Drag bucket start at C_l	0.2	0.125	0.1	0.38					
14	Drag bucket ends at C_l	0.75	0.96	0.8	1.38					
SUM :						17.3	19.4	16.7	19.8	

TABLE 4.5: Airfoil Matrix.

control surface's design and behavior.

4.3.4 Wing

This unmanned aerial vehicle (UAV) wing has been designed based on a thorough benchmarking study with other UAV wings of similar specifications. The selection of a taper ratio of 0.398 from the wing parameter 4.6 was made after analyzing the induced drag factor versus taper ratio and aspect ratio graph in Snorri's book. According to the graph 4.10, taper ratios in the range of 0.3 to 0.4 offer the most optimal point where induced drag is at its lowest. Furthermore, the dihedral angle of 5° was carefully selected to ensure stability. By applying this angle, it helps to reduce the instability in spiral mode, which can be a critical factor in UAV wing design. This stability factor is crucial to ensure that the UAV wing is safe and performs as expected while in operation. For the wing planform, LE straight taper was also chosen because, according to [20], leading edge straight taper offers the advantages of improving the aerodynamic efficiency, structural, and it may offer advantageous if it is foreseen that the operational CG will be too far forward. Based on the Figure 4.11 that the wing can achieve CL max around 1.73 at aoa of 20 degree before stall. The data was gathered by using XFLR5 LLT analysis at sea level altitude and free stream velocity of 36 m/s.

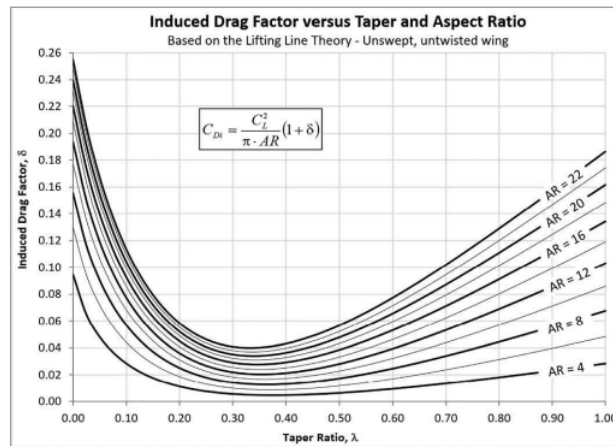


FIGURE 4.10: Induced Drag Factor versus Taper Ratio and Aspect Ratio [20].

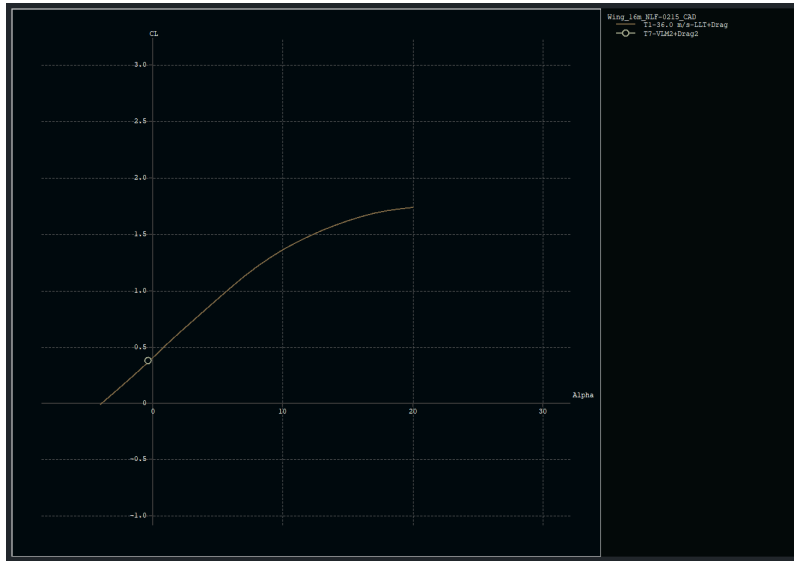


FIGURE 4.11: Estimation CL Maximum of the Wing.

Parameter	Value
Wing Area	14 m ²
Aspect Ratio	18
Span	15.96 m
Taper Ratio	0.398
Geometric Washout	-4°
Wing Incidence Angle	0°
Dihedral	5°

TABLE 4.6: Wing Parameters.

4.3.5 Tail

There are numerous options for tail configurations, starting from T-tail, H-tail, cruciform, V-tail, inverted V-tail, and so on. V-tails are one of the famous tail configurations that are being used. The reason why some use V-tails as the configuration is that it provides fewer parts and decreases the tail area [21]. One interesting case is the tail on the MQ-1 Predator, which uses an inverted V-tail. Even though it has an obvious disadvantage by limiting rotation angle, it improves lateral-directional stability. As mentioned in [20], adding a ventral fin

	Typical Values	
	Horizontal c_{HT}	Vertical c_{VT}
Sailplane	0.50	0.02
Homebuilt	0.50	0.04
General aviation—single engine	0.70	0.04
General aviation—twin engine	0.80	0.07
Agricultural	0.50	0.04
Twin turboprop	0.90	0.08
Flying boat	0.70	0.06
Jet trainer	0.70	0.06
Jet fighter	0.40	0.07 – 0.12*
Military cargo/bomber	1.00	0.08
Jet transport	1.00	0.09

TABLE 4.7: Tail Volume Table Reprinted from [23].

will improve the roll stability and stall characteristics. Instead of creating a ventral fins, the X-Tail configuration uses the area below the fuselage not just as fins but as a control surfaces. that's why X-Tails are chosen. For the sizing of the tail, tail volume sizing formula according to [22] was used for the approximation 4.1 and 4.2. The parameter S_H and l_H in eq. 4.1 and 4.2 mean the lever arm horizontal tail and vertical tail respectively, which defined as the distance between ACs wing and tail.

$$C_H = \frac{S_H \cdot l_H}{S_W \cdot c_{MAC}} \quad (4.1)$$

$$C_V = \frac{S_V \cdot l_V}{S_W \cdot b} \quad (4.2)$$

Using the Tail Volume of GA aviation single engine from table 4.7 resulted in the conventional tail parameter value 4.8, then it converted into V-Tail by using the formula 4.3 from [24].

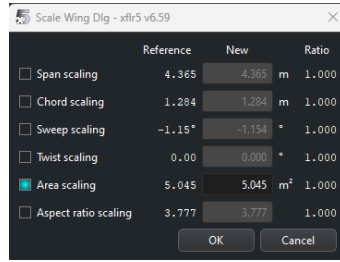
$$VTailArea = VerticalArea + HorizontalArea$$

$$VTailAngle = \tan^{-1}\left(\frac{VerticalArea}{HorizontalArea}\right) \quad (4.3)$$

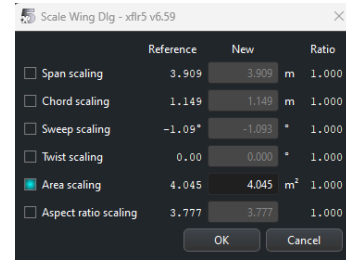
Double the size of the tail area from V-Tail 4.3 is then used for total X-Tail

	SW	CMAC	SH	LH	SV	LV	b	CH	CV
Conventional Tail	14.04	0.933	2.54709	3.6	2.496	3.6	16	0.7	0.04

TABLE 4.8: Conventional Tail Area from Tail Volume GA Single Engine.



(A) Original upper X tail area from Table ??.



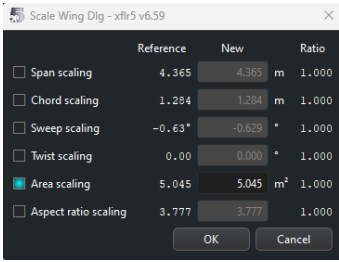
(B) Upper X tail area after iterative change by 1 m².

FIGURE 4.12: Upper X-tail.

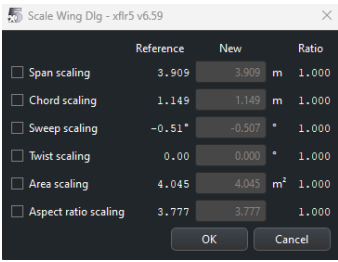
area. Double the size area from V-Tail because the 'X' shaped tail area used the area from V-Tail 4.3 for the upper section and lower section, but this size of $2 * 5.04309m^2$ only for the early approximation. The final size of tail were then adjusted for the stability purpose. After the stability anaylisis was conducted the size of the total X-tail area was decreased into $5.62m^2$ from initial size of $10.09m^2$. The Geometric shape can be seen in 4.15. The area of X-tail was decreased iteratively from the sizing result of double V-tail area start from $5.04 m^2$ as shown in Figure 4.12 to $4.04 m^2$ for the upper tail section using area scaling option in XFLR5, and it also applies for lower tail section as shown in Figure 4.13. And the result of the iterative stability analysis of the different tail area it was shown that the tail area for only upper or lower of $2.81m^2$ in Figure 4.14 makes the UAV stable in all static and dynamic modes.

	$S_{v_{tail}}$	angle (rad)	angle (deg)
Vtail (ga_{single})	5.04309	0.7803327299	44.70977204

TABLE 4.9: V-Tail Volume



(A) Original lower X tail area from Table ??.



(B) lower X tail area after iterative change by 1 m².

FIGURE 4.13: Lower X-tail.

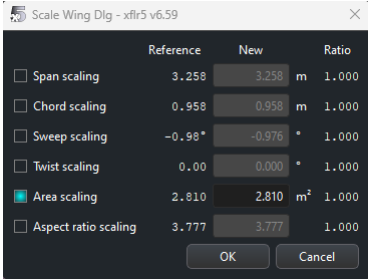


FIGURE 4.14: Final lower and upper X-tail area.

4.3.6 Total Parasite Drag

Parasite drag (CD_0) is one of the major factors that affect the movement of any object through a fluid medium, such as an aircraft. It occurs due to the resistance encountered by an object as a result of its shape and surface characteristics, rather than from the drag generated by lift. When it comes to aircraft, the concept of parasite drag is of utmost importance since it can contribute significantly to the total drag that the aircraft experiences during flight. The total parasite drag is a combination of different types of drag, such as skin friction drag, pressure drag, and interference drag. To calculate the total parasite drag of a conceptual UAV, the Open VSP tool was used. The values obtained from the tool are listed in Table 4.10. At sea level altitude with a freestream velocity of $10m/s$, the total parasite drag is 0.306824.

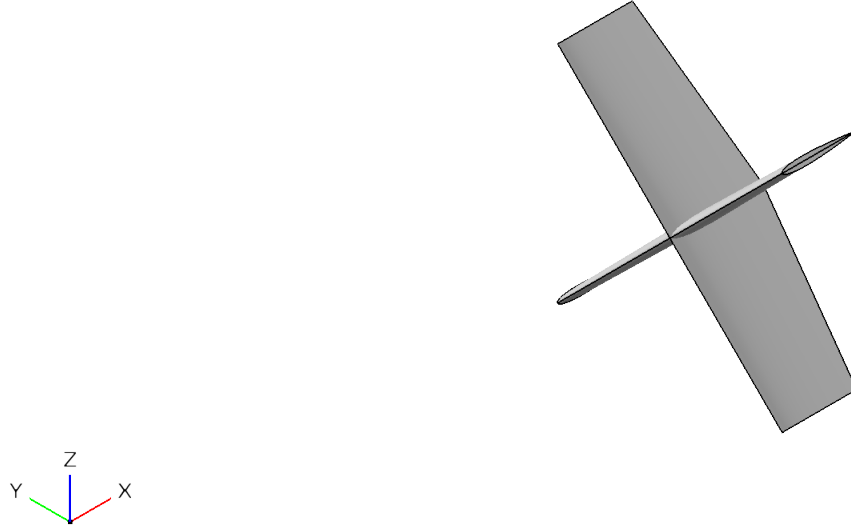


FIGURE 4.15: Geometric Shape of the X-Tail.

4.4 Static Stability Analysis

Static Stability analysis determines whether a vehicle will regain its initial condition of equilibrium after a perturbation. XFLR5 shows the results of Static Stability analysis via graphical representations of the relationship between the longitudinal static stability (pitching moment (Figure 4.16a) and lift coefficient vs α (Figure 4.16b)) and lateral-directional stability (rolling moment and sideslip angle (Figure 4.16c), and yawing moment and sideslip angle (Figure 4.16d)).

$$\text{Static Margin} = \frac{x_{np} - x_{cg}}{MAC} = -\frac{C_{m_\alpha}}{C_{L_\alpha}} \quad (4.4)$$

The result of static margin from 4.4 equation can be seen in table 4.11. This UAV exhibits the longitudinal static stability, characterized by a static margin of roughly 14%. This conceptual UAV also exhibits directional stability where

Altitude (m)	0	V_∞ (m/s)	10	S_{ref} (m^2)	14.03839
Component Name	S_{wet} (m^2)	L_{ref} (m)	f (m^2)	C_D	% Total
FuselageGeom	20.636002	8.30329	0.073844	0.00526	24.067333
WingGeom	26.945765	0.932267	0.174505	0.012431	56.874721
TAIL	4.762867	0.866013	0.029452	0.002098	9.598886
TAIL	4.693487	0.866013	0.029023	0.002067	9.45906
		Totals:	0.306824	0.021856	100

TABLE 4.10: Total Parasite Drag.

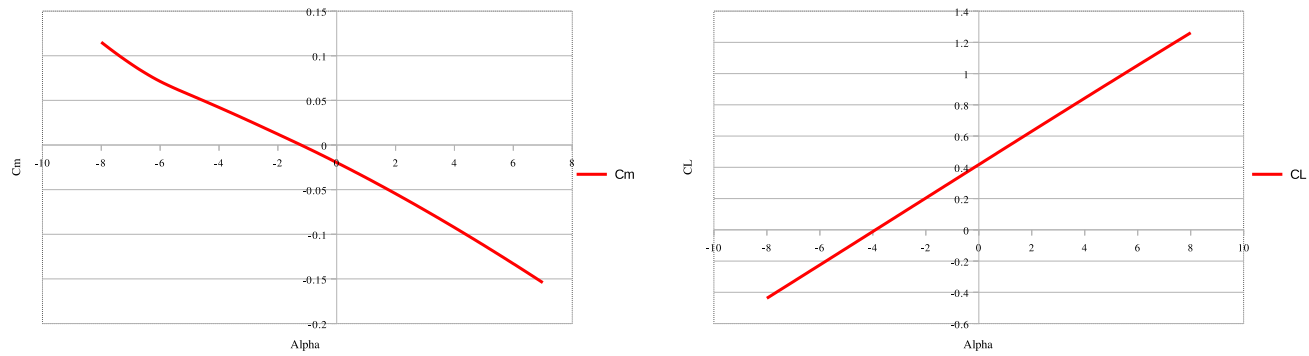
Xnp	0.549
Xcg	0.421
MAC	0.933
CMa	-0.01787475
CLa	0.106205875
Clb	-0.0011225
Cnb	0.00254925
SM	$\approx 14\%$

TABLE 4.11: Static Stability.

$Cl_\beta < 0$ and $Cn_\beta > 0$ as discussed in chapter 2.4.3.

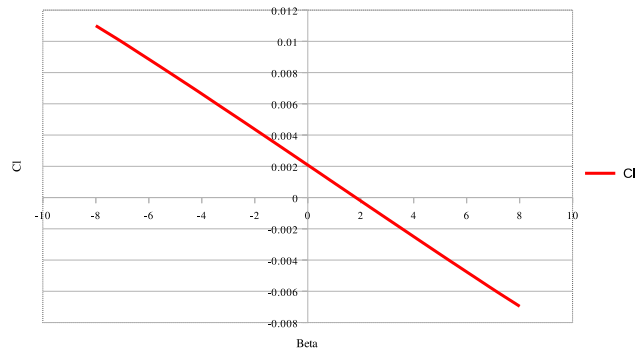
4.5 Dynamic Stability Analysis

Dynamic analysis analyze the motion aircraft over the time after it is got perturbed from its equilibrium position. The characteristic equation's roots were obtained by using type 7 analysis at cruising altitude at ≈ 7.600 meter on XFLR5 with additional parameter of extra drag from fuselage (Area : $20.64m^2$; Parasite Drag: 0.0052). The roots represents five modes of oscillation: short oscillation, phugoid, roll subsidence, dutch-roll, and spiral.

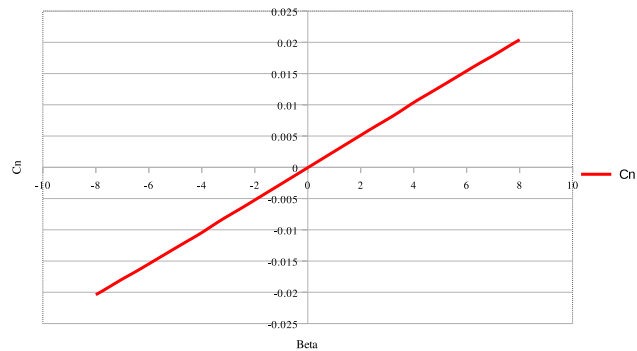


(A) Pitching Moment (C_m vs α).

(B) C_L vs α .



(c) Rolling Moment(C_l vs β).



(D) Yawing Moment (C_n vs β).

FIGURE 4.16: Static Stability.

4.5.1 Longitudinal Modes

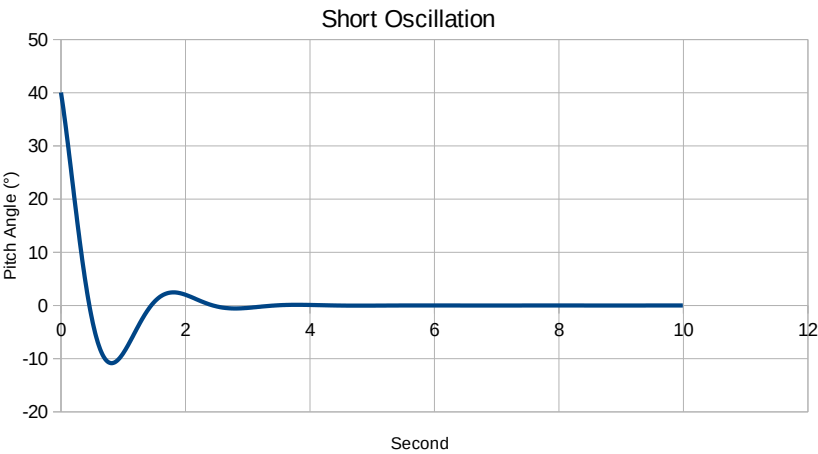
The longitudinal state matrix and roots that were obtained from XFLR5 software can be seen in equation 4.5.

$$A_{\text{long}} = \begin{bmatrix} -0.00686684 & 0.0959212 & 0 & -9.81 \\ -0.21461 & -1.73247 & 90.4096 & 0 \\ -0.000491515 & -0.111179 & -1.24764 & 0 \\ 0 & 0 & 1 & 0 \end{bmatrix} \quad (4.5)$$
$$\lambda_{1,2} = -1.491 \pm 3.162i$$
$$\lambda_{3,4} = -0.002205 \pm 0.1359i$$

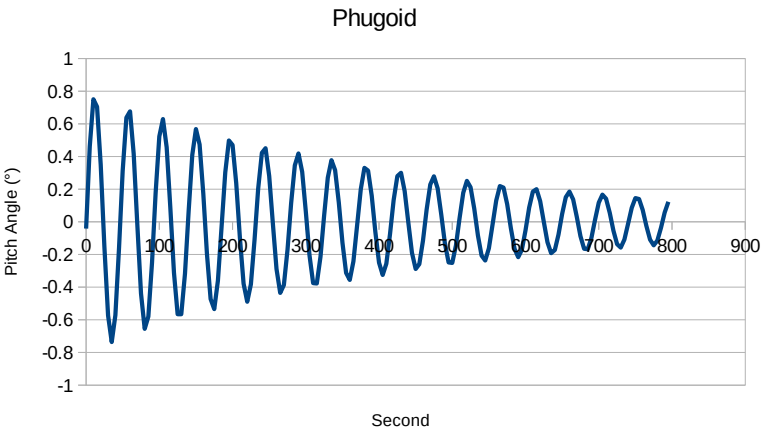
The roots $\lambda_{1,2}$ represent the short oscillation mode. Figure 4.17a shows that the aircraft is stable with a negative real value of -1.491 , which affects the damping ratio, and an imaginary value of $\pm 3.162i$, which affects the frequency. The roots produce a damping ratio value of 0.4265 and a frequency of 0.5 Hz. The damping ratio (ζ) value $0 < \zeta < 1$ indicates that the motion is oscillatory, and the frequency represents the number of completed cycles in one second.

Based on the aircraft's longitudinal modes, the phugoid mode is represented by the roots $\lambda_{3,4}$. The behavior of this mode can be observed from Figure 4.17b, which indicates that the aircraft is stable with a negative real value of -0.002205 and damping ratio of 0.0162 . This damping ratio implies that the motion is oscillatory, and is categorized as underdamped which will decay overtime. The phugoid motion has a frequency of 0.022 , which means that it completes only 0.022 cycle over one second.

It is interesting to note that both the longitudinal modes are underdamped, which means that the motion is oscillatory. However, the most visible difference between the two modes is the frequency. The phugoid motion has a lower frequency of 0.022Hz , whereas the short oscillation motion completes 0.5 cycle in one second.



(A) Short Oscillation Mode.



(B) Phugoid Mode

FIGURE 4.17: Longitudinal Modes.

4.5.2 Lateral Modes

The lateral state matrix and roots that were obtained from XFLR5 software and it can be seen in equation 4.6.

$$A_{\text{long}} = \begin{bmatrix} -0.213362 & -0.449114 & -90.7215 & -9.81 \\ -0.0668005 & -4.24284 & 0.534968 & 0 \\ 0.0897757 & -0.246755 & -0.349732 & 0 \\ 0 & 1 & 0 & 0 \end{bmatrix} \quad (4.6)$$

$$\lambda_1 = -4.317 + 0i$$

$$\lambda_{2,3} = -0.2478 \pm 2.922i$$

$$\lambda_4 = 0.006516 + 0i$$

The roots λ_1 represent the roll subsidence mode 4.18a. This mode has a negative real value of -4.317 and no imaginary value, which indicates that it is stable and will decay over time without oscillatory motion. On the other hand, the Dutch-roll mode ($\lambda_{2,3}$) has an imaginary value with a negative real value, which means it is stable and has oscillatory motion. $\lambda_{2,3}$ have damping ratio of 0.084 , which is evident from its motion in Figure 4.18b, and has a frequency of $0.465Hz$. Unfortunately, the last mode λ_4 (spiral mode) 4.18c has a positive value and no imaginary value, indicating that it is unstable and will grow overtime with no oscillatory motion.

4.5.3 S-Plane

Longitudinal Mode

$$\lambda_{1,2} = -1.491 \pm 3.162i$$

$$\lambda_{3,4} = -0.002205 \pm 0.1359i$$

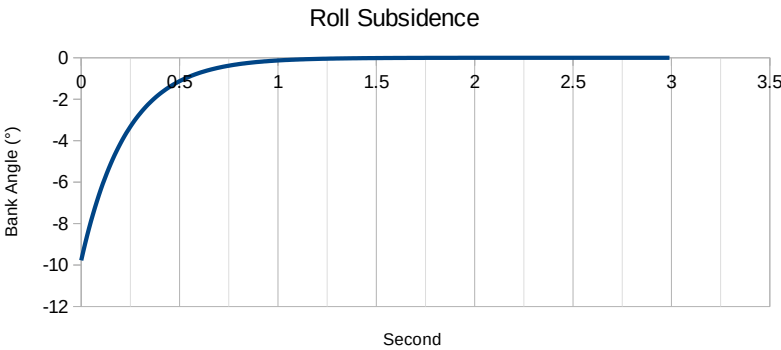
Lateral Mode

$$\lambda_1 = -4.317 + 0i$$

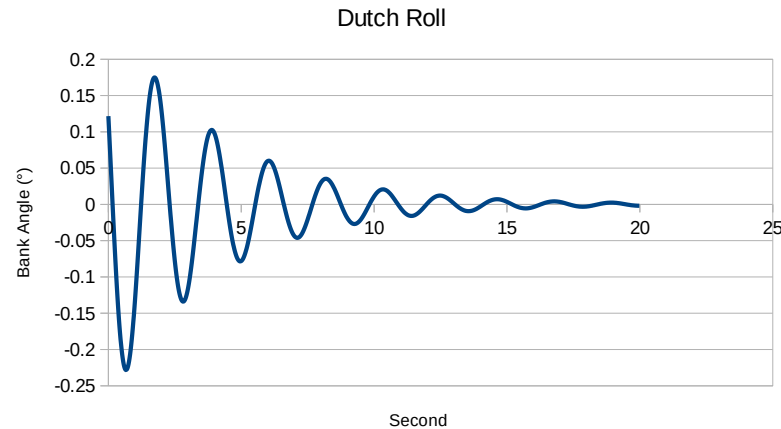
$$\lambda_{2,3} = -0.2478 \pm 2.922i$$

$$\lambda_4 = 0.006516 + 0i$$

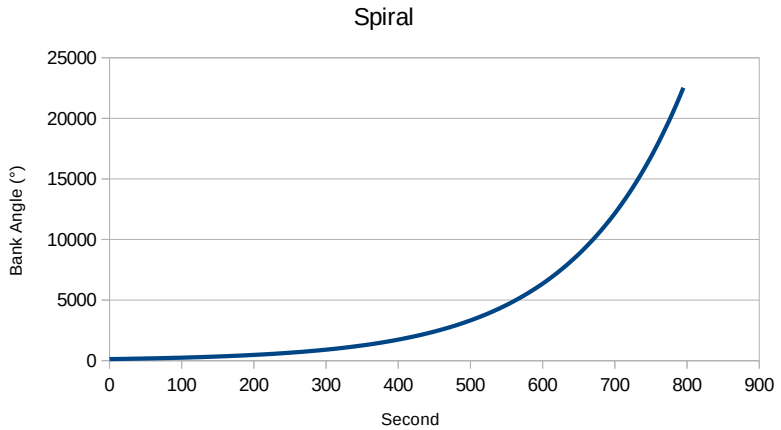
(4.7)



(A) Roll Subsidence Mode.



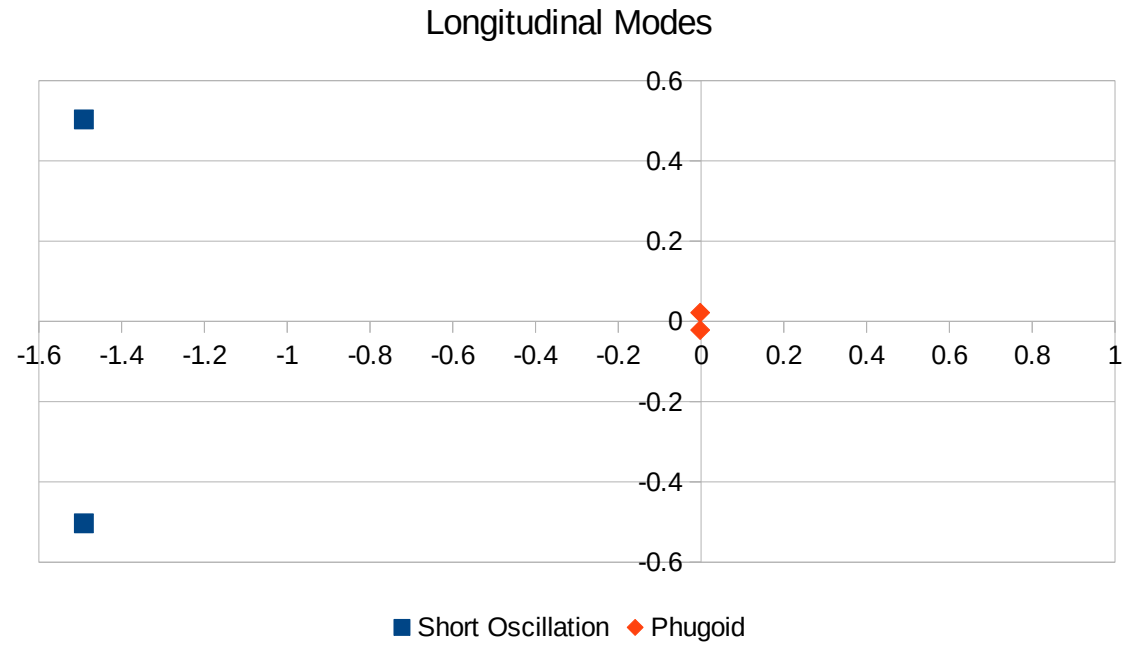
(B) Dutch-Roll Mode.



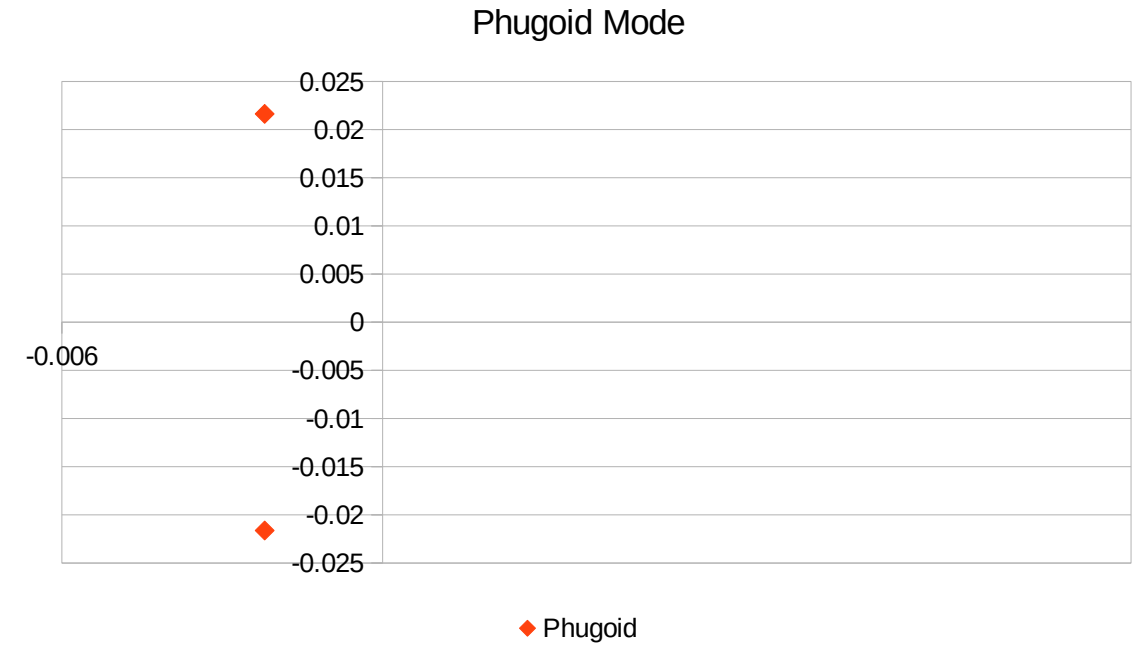
(C) Spiral Mode.

FIGURE 4.18: Lateral Modes.

The eigenvalues 4.7 represent the dynamics of a system in both the longitudinal and lateral modes. In the longitudinal mode, the complex conjugate eigenvalues $\lambda_{1,2} = -1.491 \pm 3.162i$ indicate an underdamped response with stability due to the negative real part ($\alpha = -1.491$). The second pair of eigenvalues $\lambda_{3,4} = -0.002205 \pm 0.1359i$ also signifies an underdamped response, with a real part ($\alpha = -0.002205$) very close to zero, suggesting slow damping. In the lateral mode, the eigenvalue $\lambda_1 = -4.317$ indicates a stable response with a purely real component, implying no oscillations. The negative real part ($\alpha = -0.2478$) indicates stability. The eigenvalue $\lambda_4 = 0.006516$ has a small positive real part, close to zero, suggesting a marginally unstable response in the lateral mode.

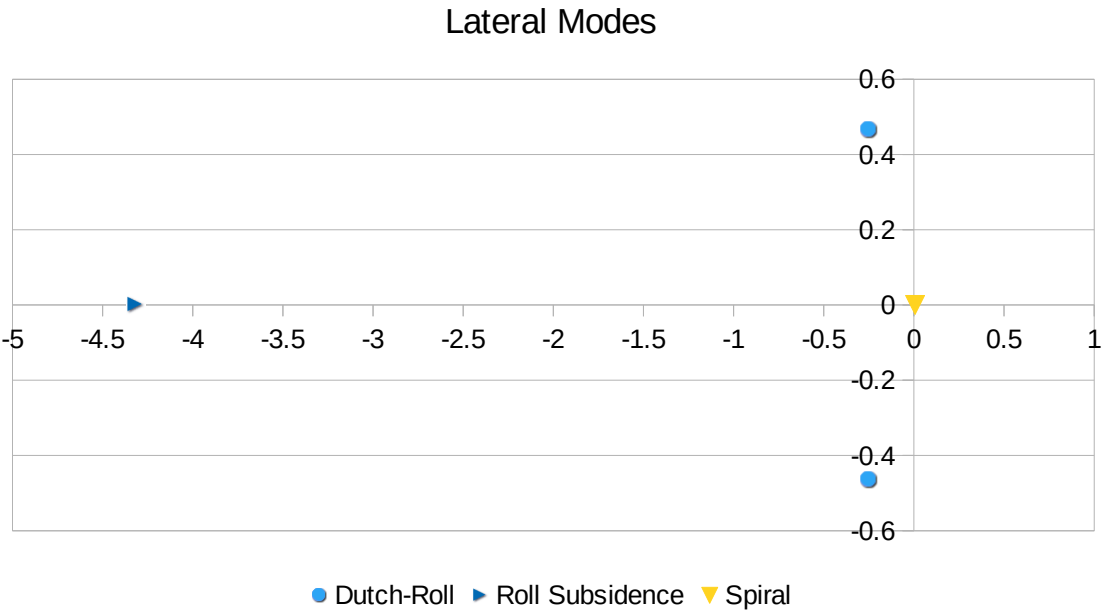


(A) Longitudinal Modes.

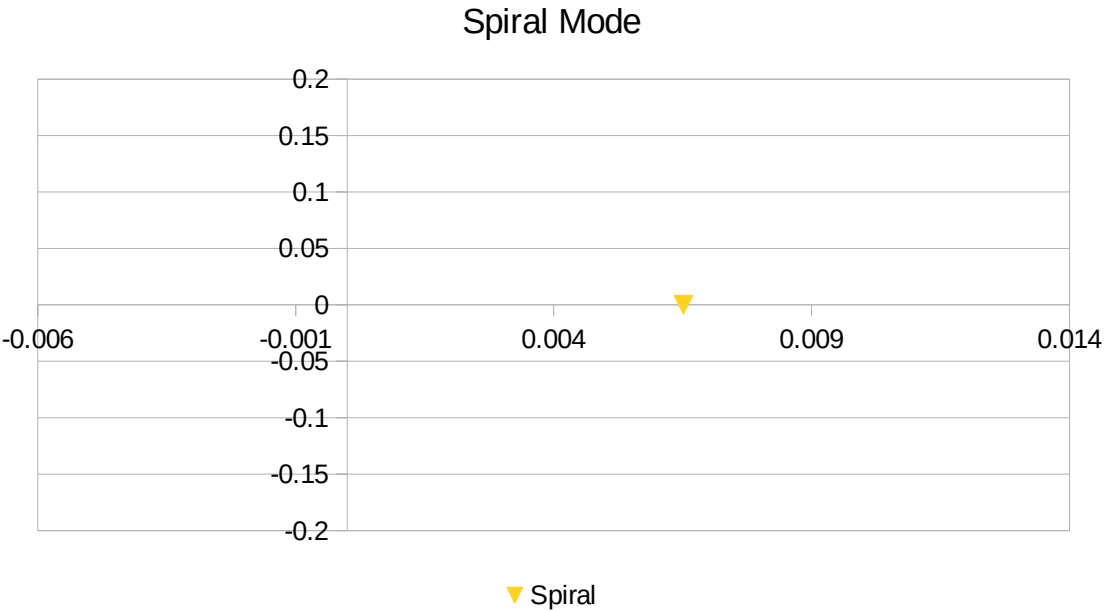


(B) Enlarged view of phugoid Mode.

FIGURE 4.19: Root Locus View of Longitudinal Modes.



(A) Lateral Modes.



(B) Enlarged view of spiral Mode.

FIGURE 4.20: Root Locus View of Lateral Modes.

CHAPTER 5

SUMMARY, CONCLUSION, RECOMMENDATION

5.1 Summary

The summary of this thesis, which based on what have been explained and analyzed, is as follows:

- In the early phase the author collected all of the data for the benchmarking study of MALE UAVs
- From benchmarking study, the payload study was conducted and concluded in 3 type of payload configurations
- The author completed the design and analysis of this conceptual MALE UAV regarding aerodynamics using Open VSP software.
- The author has analyzed not only the static but also the dynamic stability of this conceptual design by using XFLR5 software.

5.2 Conclusion

This thesis aimed to design a conceptual level MALE (Medium Altitude, Long Endurance) UAV, focusing on its aerodynamics and stability. The initial phase involved a benchmarking study that identified 22 MALE UAVs along with their specifications. However, due to the sensitive nature of MALE UAVs, some of the parameters remained unknown. The benchmarking study was followed by a payload study that resulted in the identification of different types of payload specs and two reference MALE UAVs - MQ-1 and Hermes Starliner. The payload study led to the identification of three different types of configuration- combat, ISR, and SAR missions with payloads of 456.608 kg, 283.408 kg, and 248.725 kg, respectively. Along with the configurations, the study also produced design

requirements and mission profiles. However, due to limited information on the referenced UAVs, the author modified the design requirements and mission profile based on dissertation paper [18].

The UAV's design was created using Open VSP, starting from the fuselage until the tail section. The design was then imported to CAD to create its structure by the author's colleague, Mr. Akbar, who was responsible for the structure, mission avionics, and payload system. The finished design in Open VSP was analyzed using the drag analysis function from the analysis, which resulted in each component parasite drag and total parasite drag of 0.0218. The full configuration design was then replicated in XFLR5 to assess its stability with the mass input from the structure and payloads. Based on the XFLR5 analysis, the designed wing reached its CL max 1.73 at 20 degrees aoa with the cruising altitude and the speed of 36 m/s.

The stability analysis in XFLR5 resulted in stability in all modes except spiral mode, where it is marginally small but positive, so it grows over time. The study provided critical insights into the design of MALE UAVs and will be useful for future research in the field. Based on the static stability results, this UAV fulfills the FAR 23 static stability requirements and is also stable in dynamic short-period mode and Dutch roll mode. So, basically, it should also comply with the Stanag 4671 in terms of general stability.

5.3 Recommendation

Although the current study is only conceptual design level, there is still room for further enhancements to be made. These improvements are :

- Further study about this conceptual MALE UAV's performance is needed to confirm the design requirements.
- Further study about its subsystems and payload is also needed because of the lack of available specifications on the internet.
- The different configurations or geometric shapes can also be explored to meet the design requirements.
- Further study about the control surface design of this Conceptual MALE UAV is needed because this thesis does not cover the control surface design.

Bibliography

- [1] W. H. Frederick and Library of Congress, Eds., *Indonesia: A Country Study* (Pamphlet / Department of the Army 550-39), 5. ed., 1. print., research completed November 1992. Washington, DC: U.S. Government Printing Office, 1993, ISBN: 978-0-8444-0790-6.
- [2] N. Nurdin, *Hanya ada 13.466 Pulau di Indonesia*.
- [3] D. Indonesia, *Indonesia Introduced BLACK EAGLE, Unmanned Aircraft*, Jan. 2020. (visited on 01/27/2024).
- [4] CNN, *BPPT Pamer Drone Buatan Indonesia*, News, Dec. 2019.
- [5] B. P. Tice, "UNMANNED AERIAL VEHICLES - The FOrce Multiplier of the 1990s,"
- [6] M. Hassanalian and A. Abdelkefi, "Classifications, applications, and design challenges of drones: A review," *Progress in Aerospace Sciences*, vol. 91, pp. 99–131, May 2017, ISSN: 03760421. DOI: [10.1016/j.paerosci.2017.04.003](https://doi.org/10.1016/j.paerosci.2017.04.003). (visited on 01/27/2024).
- [7] R. E. Weibel, "Safety Considerations for Operation of Different Classes of Unmanned Aerial Vehicles in the National Airspace System,"
- [8] J. P. Fielding, *Introduction to Aircraft Design* (Cambridge Aerospace Series 11), 12. printing. Cambridge: Cambridge Univ. Press, 2010, Literaturverz. S. [259] - 260, ISBN: 978-0-521-65722-8 978-0-521-44319-7.
- [9] J. D. Anderson, *Fundamentals of Aerodynamics* (McGraw-Hill Series in Aeronautical and Aerospace Engineering), Sixth edition. New York, NY: McGraw-Hill Education, 2017, Literaturverzeichnis Seite 1111-1116, ISBN: 978-1-259-12991-9.
- [10] M. V. Cook, *Flight Dynamics Principles : A Linear Systems Approach to Aircraft Stability and Control*. Elsevier Science, 2011.

- [11] M. H. Sadraey, *Design of Unmanned Aerial Systems*, 1st ed. Wiley, Mar. 2020, ISBN: 978-1-119-50870-0 978-1-119-50861-8. DOI: [10.1002/9781119508618](https://doi.org/10.1002/9781119508618). (visited on 02/01/2024).
- [12] T. S. Sugandi, Nathan, S. K. Subrata, O Arifianto, and M. A. Moelyadi, "Prediction of static stability in tandem wing unmanned aerial vehicle," *Journal of Physics: Conference Series*, vol. 1130, p. 012 028, Nov. 2018, ISSN: 1742-6588, 1742-6596. DOI: [10.1088/1742-6596/1130/1/012028](https://doi.org/10.1088/1742-6596/1130/1/012028). (visited on 01/28/2024).
- [13] J. D. Anderson, *Introduction to Flight* (Anderson Series), 7. ed. New York, NY: McGraw-Hill, 2012, Includes bibliographical references and index, ISBN: 978-0-07-338024-7 978-0-07-108605-9.
- [14] P. Panagiotou, P. Kaparos, C. Salpingidou, and K. Yakinthos, "Aerodynamic design of a MALE UAV," *Aerospace Science and Technology*, vol. 50, pp. 127–138, Mar. 2016, ISSN: 12709638. DOI: [10.1016/j.ast.2015.12.033](https://doi.org/10.1016/j.ast.2015.12.033). (visited on 01/26/2024).
- [15] Z. Goraj, "PW-125 MALE UAV Design Project Developed in Warsaw University of Technology," in *AIAA 3rd "Unmanned Unlimited" Technical Conference, Workshop and Exhibit*, Chicago, Illinois: American Institute of Aeronautics and Astronautics, Sep. 2004, ISBN: 978-1-62410-081-9. DOI: [10.2514/6.2004-6326](https://doi.org/10.2514/6.2004-6326). (visited on 01/26/2024).
- [16] A. Karki, K. Darlami, and S. Bhattra, "Conceptual design and stability analysis of a fixed wing uas research platform for aerial experiments," Oct. 2021.
- [17] A. Septiyana, K. Hidayat, A. Rizaldi, *et al.*, "Analysis of aerodynamic characteristics using the vortex lattice method on twin tail boom unmanned aircraft," in *PROCEEDINGS OF THE 3RD INTERNATIONAL SEMINAR ON METALLURGY AND MATERIALS (ISMM2019): Exploring New Innovation in Metallurgy and Materials*, Tangerang Selatan, Indonesia, 2020, p. 020 003. DOI: [10.1063/5.0002337](https://doi.org/10.1063/5.0002337). (visited on 01/26/2024).

- [18] Clarke, Adrian James, “The conceptual design of novel future UAV’s incorporating advanced technology research components,” Ph.D. dissertation, Cranfield University. (visited on 10/11/2023).
- [19] R. A. McDonald and J. R. Gloudemans, “Open Vehicle Sketch Pad: An Open Source Parametric Geometry and Analysis Tool for Conceptual Aircraft Design,” in *AIAA SCITECH 2022 Forum*, San Diego, CA & Virtual: American Institute of Aeronautics and Astronautics, Jan. 2022, ISBN: 978-1-62410-631-6. DOI: [10.2514/6.2022-0004](https://doi.org/10.2514/6.2022-0004). (visited on 01/27/2024).
- [20] S. Gudmundsson, *General Aviation Aircraft Design: Applied Methods and Procedures*, Second edition. Oxford Cambridge, MA: Butterworth-Heinemann, 2022, ISBN: 978-0-12-818465-3.
- [21] J. Gundlach and S. Merkowitz, *University of Washington Big G Measurement*. [Online]. Available: https://asd.gsfc.nasa.gov/Stephen.Merkowitz/G/Big_G.html.
- [22] D. Scholz, “Empennage sizing with the tail volume complemented with a method for dorsal fin layout,” *INCAS BULLETIN*, vol. 13, no. 3, pp. 149–164, Sep. 2021, ISSN: 22474528, 20668201. DOI: [10.13111/2066-8201.2021.13.3.13](https://doi.org/10.13111/2066-8201.2021.13.3.13). (visited on 01/29/2024).
- [23] D. P. Raymer, *Aircraft Design: A Conceptual Approach* (AIAA Education Series), Sixth edition. Reston, VA: American Institute of Aeronautics and Astronautics, Inc, 2018, Includes bibliographical references and index, ISBN: 978-1-62410-490-9.
- [24] M. Drela, *Quick V-Tail Sizing*.

Appendices

Appendix A

.1 Dynamic Stability Output

xflr5 v6.59

01.02.2024 18:17:40

Launching Analysis

Launching the 3D Panel Analysis....

Wing_16m_NLF-0215_CAD

Type 7 - Stability polar

Wings as thin surfaces

Using ring vortices - VLM2

Using Neumann boundary conditions for wings

Density = 0.65969kg/m³

Viscosity = 2.4113e-05m²/s

Reference Area = 13.985m²

Reference length = 15.919m

Counted 1234 panel elements

Solving the problem...

Calculation for control position 0.00

Mass= 1493.644 kg

___Center of Gravity Position - Body axis___

CoG_x= 0.4213 m

CoG_y= 0.0794 m

CoG_z= 0.1152 m

___Inertia - Body Axis - CoG Origin___

Ibxx= 8074 kg.m²

Ibyy= 3170 kg.m²

Ibzz= 1.11e+04 kg.m²

Ibxz= 95.61 kg.m²

Creating the unit RHS vectors...

Creating the influence matrix...

Performing LU Matrix decomposition...

Solving the LU system...

Time for linear system solve: 0.720 s

Searching for zero-moment angle... Alpha=-0.35429°

Creating source strengths...

Calculating doublet strength...

Calculating speed to balance the weight...VInf = 91.56865 m/s

___Inertia - Stability Axis - CoG Origin___

Isxx= 8075

Isyy= 3170

Iszz= 1.11e+04

Isxz= 114.3

Calculating the stability derivatives

Creating the RHS translation vectors

LU solving for RHS - longitudinal

Calculating forces and derivatives - lateral

Creating the RHS rotation vectors

LU solving for RHS - lateral

Calculating forces and derivatives - lateral

No active control - skipping control derivatives

Longitudinal derivatives

Xu=	-10.257	Cxu=	-0.024282
Xw=	143.27	Cxa=	0.33918
Zu=	-320.55	Czu=	-0.0012181
Zw=	-2587.7	CLa=	6.1261
Zq=	-1731.2	CLq=	8.787
Mu=	-1.5583	Cmu=	-0.0039547
Mw=	-352.49	Cma=	-0.89454
Mq=	-3955.6	Cmq=	-21.522
Neutral Point position=	0.55753 m		

Lateral derivatives

Yv=	-318.69	CYb=	-0.75446
Yp=	-670.82	CYp=	-0.19952
Yr=	1265.3	CYr=	0.37634
Lv=	-549.67	Clb=	-0.081744
Lp=	-34233	Clp=	-0.63959
Lr=	4359.8	Clr=	0.081457
Nv=	1003.8	Cnb=	0.14929
Np=	-2253.2	Cnp=	-0.042097
Nr=	-3942	Cnr=	-0.073651

-----State matrices-----

Longitudinal state matrix

-0.00686684	0.0959212	0	-9.81
-------------	-----------	---	-------

-0.21461	-1.73247	90.4096	0
-0.000491515	-0.111179	-1.24764	0
0	0	1	0

Lateral state matrix

-0.213362	-0.449114	-90.7215	9.81
-0.0668005	-4.24284	0.534968	0
0.0897757	-0.246755	-0.349732	0
0	1	0	0

___Longitudinal modes___

Eigenvalue: -1.491+-3.162i | -1.491+3.162i | -0.002205+-0.1359i | -0.002205+ 0.1359i

 Eigenvector: 1+0i | 1+ 0i | 1+0i | 1+ 0i

55.86+-42.47i | 55.86+42.47i | -0.02563+ 0.001542i | -0.02563+-0.001542i

-1.334+-2.067i | -1.334+2.067i | 0.001886+6.803e-05i | 0.001886+-6.803e-05i

0.6975+-0.09293i | 0.6975+0.09293i | -0.0007258+0.01387i | -0.0007258+-0.01387i

___Lateral modes___

Eigenvalue: -4.317+0i | -0.2478+-2.922i | -0.2478+2.922i | 0.006516+0i

 Eigenvector: 1+0i | 1+0i | 1+0i | 1+0i

0.736+0i | -0.01286+-0.005153i | -0.01286+ 0.005153i | 0.01472+0i

0.02315+0i | 0.0006731+0.03178i | 0.0006731+ -0.03178i | 0.2418+0i

-0.1705+0i | 0.002121+-0.004221i | 0.002121+ 0.004221i | 2.259+0i

Calculating aerodynamic coefficients in the far field plane

Calculating point -0.35°....

Computing On-Body Speeds...
Computing Plane for alpha= -0.35°
Calculating aerodynamic coefficients...
Calculating wing...Main Wing
Calculating wing...Elevator
Calculating wing...Fin

Phillips formulae:

Phugoid eigenvalue: -0.00129+ 0.13749i
frequency: 0.022 Hz
damping: 0.009
Dutch-Roll eigenvalue: -0.24954+ 2.95373i
frequency: 0.472 Hz
damping: 0.084

-----Finished operating point calculation for control position 0.00-----

.2 Benchmarking Table

A CONCEPTUAL DESIGN OF FLEXIBLE MISSION MALE: AERODYNAMICS AND STABILITY

No	Aircraft Name	Country of Origin	Flight Status	Compliance to NATO STANAG 4671	Military/Civilian/Both	MTOW (kg)
1	Yabhon United 40	UAE	Yes		Military	1,500
2	Vestel Karayel	Turkey	Yes	Yes?	Military	560
3	TAI Anka	Turkey	Yes		Military	1,600
4	Shahed 129	Iran	Yes	No	Military	990
5	Northrop Grumman Firebird	USA	Yes		Military	2,268
6	Kronshtadt Orion	Russian	Yes		Military	1,150
7	KAL KUS-FS	South Korea	Yes		Both	5,750
8	INTA Milano	Spain	Yes		Military	-
9	IAIO Fotros	Iran	Yes		Military	3,500
10	IAI Heron	Israel	Yes		Military	1,270
11	HCUAV RX-1	Greece			Civilian	185
12	HAI Pegasus II	Greece	Yes		Military	250
13	General Atomics MQ-1 Predator	USA	Yes		Military	1,020
14	Falco Explorer	Italy	No		Military	1,300
15	Eurodrone	Europe	No		Military	11,000
16	Elbit Hermes 900	Israel	Yes	No	Military	1,180
17	EADS Talarion	Europe/Turkey	No		Military	10,000
18	DRDO Rustom-1	India	Yes		Military	720
19	Denel Dynamics Bateleur	South Africa	Yes		Military	1000
20	Baykar Bayraktar TB2	Turkey	Yes		Military	700
21	Aeronautics Defense Dominator	Israel	Yes		Military	1,900
22	Elbit Hermes Starliner	Israel	Yes	Yes	Civilian	1,600
23	Gaillard ASA 1204 AAROK	France	No		Both	5,500

A CONCEPTUAL DESIGN OF FLEXIBLE MISSION MALE: AERODYNAMICS AND STABILITY

No	Aircraft Name	EMTOW (kg)	Payload Mass (kg)	Fuel Mass (kg)	A/C Dimensions		Wing Area (m ²)	Wing Span (m)	Aspect Ratio	Engine Name
					Length (m)	Height (m)				
1	Yabhon United 40	520	1,000	225	20	4.38	24	18	13.50	1x Rotax 914 UL Piston, 1x Electric Motor
2	Vestel Karayel	475	50	-	6.5	2.45		13	#DIV/0!	Unspecified
3	TAI Anka	700	-	-	8	3.4		17.3	#VALUE!	1x Thielert Centurion 2.0 Turbocharged
4	Shahed 129	-	400	-	6	3.1		10.5	#DIV/0!	1x Rotax 914
5	Northrop Grumman Firebird	-	560	-	10	3		24.1	#DIV/0!	Lycoming TEO-540
6	Kronshtadt Orion	500	250	-	8	2		16	#DIV/0!	APD110/ 120 Engine (Prototype- Rotax 914)
7	KAL KUS-FS	-	-	-	10	3		16	#DIV/0!	1x Hanwha Aerospace Turboprop
8	INTA Milano	900	150	-	8.2			12.5	#DIV/0!	1x Turbocharged boxer engine
9	IAIO Fotros	520	-	-	8.25	1.86		49	#DIV/0!	Unknown
10	IAI Heron	-	470	-	8.5			16.6	#DIV/0!	1x Rotax 914
11	HCUAV RX-1	95	35	55	4.035			6.4	#DIV/0!	Unspecified
12	HAI Pegasus II	200	50	-	4.3			6.2	#DIV/0!	
13	General Atomics MQ-1 Predator	513	120	387	8.23	2.1	11.45	14.8	19.13	Rotax 914F
14	Falco Xplorer	950	350		9			18.8	#DIV/0!	
15	Eurodrone	8,700	2,300		16			30	#DIV/0!	General Electric Catalyst
16	Elbit Hermes 900	830	350		8.3			15	#DIV/0!	Rotax 914
17	EADS Talarion	3,200	6,800		10	3.45		28	#DIV/0!	
18	DRDO Rustom-1	625	95		5.12	2.4		7.9	#DIV/0!	Lycoming O-320
19	Denel Dynamics Bateleur	800	200					15	#DIV/0!	Rotax 914 or Subaru EA-82
20	Baykar Bayraktar TB2	550	150	237	6.5	2.2		12	#DIV/0!	Rotax 912-iS
21	Aeronautics Defense Dominator	1,527	373	231	8.56	2.49		13.55	#DIV/0!	Lycoming Engine AE300 Turbocharged
22	Elbit Hermes Starliner	1,150	450					17	#DIV/0!	Rotax 914 (HFE)
23	Gaillard ASA 1204 AAROK	2,500	2,721.55					22	#DIV/0!	

A CONCEPTUAL DESIGN OF FLEXIBLE MISSION MALE: AERODYNAMICS AND STABILITY

No	Aircraft Name	Engine Type (Turboprop/Turbojet/Turbopfan)	Propeller Diameter (if turboprop) (m)	Number of Blade (if turboprop)	Number of Engines	Max (Thrust/Power) of One Engine (N/kw)	Total Thrust/Power (N/kw)	T/W	W/S (N/m ²)	Wing Position (High, Mid, Low)	Type of Tail	Retractable Landin Gear
1	Yabhon United 40	Piston	3.96	3	2	84.58 + 58.84	143.0	0.095	613.125	High (Tandem)	Conventional	Yes
2	Vestel Karayel	Piston	1.45	2	1	72.0	72.0	0.129		High	Conventional	No
3	TAI Anka	Piston		3	1	115.6	116.0	0.073		High	V tail	Yes
4	Shahed 129	Piston		3	1	75.0	75.0	0.076		High	V tail	Yes
5	Northrop Grumman Firebird	Piston		5		261.0	261.0	0.115		High	Twintail-Boom	Yes
6	Kronshtadt Orion	Piston		2	1	84.6	84.6	0.074		Low	V tail	Yes
7	KAL KUS-FS	Turboprop		4	1	882.6	882.6	0.016		Low	V tail	Yes
8	INTA Milano	Piston		3	1			#VALUE!		Low	V tail	No
9	IAIO Fotros	Piston		2				0.000		High	Twintail-Boom	Yes
10	IAI Heron	Piston		3	1	84.6	84.6	0.067		High	Twintail-Boom	Yes
11	HCUAV RX-1	Piston		2	1	18	18	0.099		High	Inverted - Vtail-Boom	No
12	HAI Pegasus II	Piston		2				0.000		High	Twintail-Boom	No
13	General Atomics MQ-1 Predator	Piston		2	1	85	85	0.083		Mid	V-Tail Inverted	No
14	Falco Xplorer			2				0.000		High	V-tail	
15	Eurodrone	Turboprop		6	2			0.000		Low	T-Tail	Yes
16	Elbit Hermes 900	Piston		2	1	86	86	0.073		Mid	V-tail	Yes
17	EADS Talarion	Turbojet			2			0.000		Mid	Conventional	Yes
18	DRDO Rustom-1	Piston		3	1			0.000		Mid	Winglet	No
19	Denel Dynamics Bateleur	Piston		3	1			0.000		Mid	H-Tail	
20	Baykar Bayraktar TB2	Piston		2	1			0.000		Low	V tail inverse	No
21	Aeronautics Defense Dominator	Piston	1.4	3	2			0.000		Low	T-Tail	Yes
22	Elbit Hermes Starliner	Piston		3	1			0.000		Mid	V tail	Yes
23	Gaillard ASA 1204 AAROK											

A CONCEPTUAL DESIGN OF FLEXIBLE MISSION MALE: AERODYNAMICS AND STABILITY

No	Aircraft Name	TakeOff Distance (m)	Landing Distance (m)	Vmax (m/s)	Mach Max (M) *20°C	V Cruise (m/s)	V Stall (m/s)	Range (km)	Ferry Range (km)	Service Ceiling (m)	Airfoil	Wing Sweep Angle (deg)	Dihedral/U nhedral
1	Yabhon United 40	550	400	61	0.178	21	14			7,000			
2	Vestel Karayel	500	750	42	0.121	32		2,255		6,900			
3	TAI Anka	350	600	60	0.176			4,900		9140			
4	Shahed 129			49	0.142	42		1,700	3,400	7,300			
5	Northrop Grumman Firebird			103	0.300					7,600			Dihedral
6	Kronshtadt Orion			63	0.182	33		1440		7,500			
7	KAL KUS-FS			257	0.749			500		13,716			
8	INTA Milano			120	0.350					7,800			
9	IAIO Fotros			111	0.324	96		4000		7,620			
10	IAI Heron			58	0.168			350		10,000	IAI SA-21		
11	HCUAV RX-1			53	0.154	44	19	150>		2000			
12	HAI Pegasus II			44	0.130			2000					
13	General Atomics MQ-1 Predator			60	0.176	38		1250		7,600			
14	Falco Xplorer				0.000					9,100			
15	Eurodrone				0.000	139				13,700			
16	Elbit Hermes 900			31	0.091				9000	9,100			
17	EADS Talarion			175	0.510			16000		15,000			
18	DRDO Rustom-1			42	0.121	35		250	1000	8,000			
19	Denel Dynamics Bateleur			69	0.202			750		8,000			
20	Baykar Bayraktar TB2	400	400	61	0.178			300		7,620			Dihedral
21	Aeronautics Defense Dominator	649	647	102	0.297	90	32	2,269		9,100			
22	Elbit Hermes Starliner				0.000					9,144			Dihedral
23	Gaillard ASA 1204 AAROK					129				9,144			

Turnitin Report

Alibananda Thesis

ORIGINALITY REPORT

17%

SIMILARITY INDEX

14%

INTERNET SOURCES

12%

PUBLICATIONS

9%

STUDENT PAPERS

PRIMARY SOURCES

1	aerocastle.files.wordpress.com Internet Source	3%
2	zombiedoc.com Internet Source	1%
3	web.archive.org Internet Source	1%
4	karya.brin.go.id Internet Source	1%
5	mafiadoc.com Internet Source	1%
6	www.scientificbulletin.upb.ro Internet Source	1%
7	T S Sugandi, Nathan, S K Subrata, O Arifianto, M A Moelyadi. "Prediction of static stability in tandem wing unmanned aerial vehicle", Journal of Physics: Conference Series, 2018 Publication	<1%
8	www.scribd.com Internet Source	<1%

Curriculum Vitae



Basic Information	
Name	Alibananda Tito Ash Shidiqi
Place of Birth	Bandar Lampung, Indonesia
Date of Birth	04, 08, 1999
Address	Citra Pemuda Regency No.14A, Cirebon, Jawa Barat, Indonesia
Year	Education
2020 - present	International University Liaison Indonesia (IULI)
2018 - 2019	Studienkolleg Hamburg
2015 - 2017	Hayatan Thayyibah Senior High School
2013 - 2015	Al-Azhar Cirebon Junior High School
2008 - 2013	Al-Azhar Cirebon Elementary School
Year	Courses
2017 - 2018	German Language Courses (A1-B2) Class
Year	Seminars & Workshops
2022	Basic Aircraft Maintenance Training
Year	Organizational Experiences Experiences
2015 - 2016	Member of LIPOSIS (Lingkaran Persatuan Osis Sukabumi)
2016	Member of Hayatan Thayyibah Senior High School Student Council
2021 - 2022	Member of Event Management in Aviation Engineering Student Association